An Automated Segmentation of Retinal Images for use in Diabetic Retinopathy Studies

By

Daniel Moges Tadesse

A thesis submitted in partial fulfillment of the requirements for the Degree of Master of Science in Biomedical Engineering

Center of Biomedical Engineering

Addis Ababa Institute of Technology

Addis Ababa University

Advisor: Dawit Assefa (PhD.)

Co-Advisors: Birhanu Assefa (MSc.)

Tedla Kebede (M.D.)

Addis Ababa, Ethiopia, October 2014

Declaration

I, the undersigned, declare that this thesis is my original work. It has never been presented for a degree in any other institution and that all sources of materials used in it have been duly acknowledged.

Name: _____

Signature: _____

Date: _____

This MSc. thesis has been submitted for examination with my approval as an advisor.

_____

Dawit Assefa Haile (PhD.)

Addis Ababa University

School of Graduate Studies

Certificate of Examination

This is to certify that the thesis prepared by Daniel Moges entitled*: An Automated Segmentation of Retinal Images for use in Diabetic Retinopathy Studies* submitted in partial fulfillment of the requirements for the degree of Master of Science in Biomedical Engineering (Bioinstrumentation and Imaging) complies with the regulations of the University and meets the accepted standards with respect to originality and quality.

Signed by the examining committee

Examiner _____Signature _____ Date _____

Examiner _____Signature _____ Date _____

Examiner _____Signature _____ Date _____

Advisor _____Signature _____ Date _____

_____

Chief of Department or Graduate program coordinator

Abstract

An Automated Segmentation of Retinal Images for use in Diabetic Retinopathy Studies

Daniel Moges
Addis Ababa University, 2014

Automated computer aided detection of retinal lesions associated with Diabetic Retinopathy (DR) offers many potential benefits. In a screening setting, it allows the examination of large number of images in less time and more objectively than traditional observer driven techniques. In a clinical setting, it can be an important diagnostic aid by reducing the workload of trained graders and other costs. However, the segmentation of major pathological structures and their subsequent follow–ups are not easy because of various artifacts such as presence of anatomical structures with highly correlated pixels with that of lesion, illumination variability, noise and movement of the eye during multiple visits by the patient. This study presents a novel mathematical scheme for analysis of color retinal images acquired through digital fundus cameras from patients treated for DR. The proposed scheme uses a holistic representation of the color images in the three (trinion) space and applies trinion based Fourier transforms to extract useful imaging features for the purpose of classification and segmentation of retinal images. A suitable color space transformation and a way of extracting robust higher order features are included in the method. The scheme has been applied in analyzing images acquired from standard retinal image databases. Results have showed that the algorithm achieved 86.06% sensitivity, 96.06% specificity, and 92.65% accuracy for pixel base segmentation of Hard Exudates (HEs) - the most prevalent lesions that appears in the earliest stages of DR, while it achieved 96.67% sensitivity, 100% specificity and 97.3% accuracy for image base classification of abnormalities due to DR.

Acknowledgement

It is a pleasure to thank the many people who made this thesis possible. First and foremost I would like to express my special appreciation and thanks to my advisor Dr. Dawit Assefa (PhD.), you have been a tremendous mentor for me. I would like to thank you for encouraging my research and for allowing me to see things in different directions. Your patience, motivation, enthusiasm, and immense knowledge and advice on both researches as well as on my career have been priceless. I would also like to thank my co-advisors Birhanu Assefa (MSc.) and Dr. Tedla Kebede (M.D.), your efforts have been supportive since the day I began working on the thesis ideas.

I am also grateful to Dr. Masreshaw Demelash (PhD.), PG coordinator, for all his help and encouragement. A special thanks to my mom, brothers and sisters, for their countless support, love and patience. Finally I am grateful to all my friends who incented me to strive towards my goal.

Table of Contents

List of tables

List of figures

Acronyms

ACC	Accuracy
AMD	Age-related Macular Degeneration
CBIR	Content Based Image Retrieval
CLAHE	Contrast Limited Adaptive Histogram Equalization
CP	Cluster Prominence
CW	Cotton Wool
DME	Diabetic Macular Edema
DR	Diabetic Retinopathy
DRIVE	Digital Retinal Image for Vessel Extraction
EX	Exudate
FT	Fourier Transform
FROC	Free Response Operating Curve
GLCM	Gray Level Co-occurrence Matrix
H	Hemorrhage
HE	Hard Exudate
HRF	High Resolution Fundus image
HOS	Higher Order Statistics
ICA	Independent Component Analysis
KNN	K- Nearest Neighborhood
LDA	Linear Discriminant Analysis
MA	MicroAneurysms
OCT	Optical Coherence Tomography

OD	Optic Disk
PCA	Principal Component Analysis
PPV	Positive Predictive Value
SEx	Soft Exudates
SE	Sensitivity
SP	Specificity
SVM	Support Vector Machine
STARE	STructured Analysis of the REtina
TFT	Trinion Fourier Transform

Chapter one

1. Introduction

1.1. Background

The retina is an interior surface of the human eye which acts as the film of the eye. It converts light rays into electrical signals and sends them to the brain through the optic nerve. The optic nerve is the cable connecting the eye to the brain. The optic disc (OD) is the bright region within the retinal image. It is the spot on the retina where the optic nerve leaves and blood vessels enter the eye. The macula is a small area near the central part of the retina which is responsible for central light vision. The fovea is an indentation in the centre of the macula. This small part of the retina is responsible for highest visual acuity. The vascular network supplies oxygen, nutrients, and blood to the retina [1].

The major leading causes of blindness and visual impairment that affect human eyes are DR, glaucoma, age-related macular degeneration (AMD) and cataract. Cataract affects the front of the eye (clouding of the lens), while the remaining three diseases affect the retina and/or optic nerve head at the back of the eye. An important difference between cataract and the other three eye diseases is that cataract is usually noticed by the patient early enough for adequate treatment, while the early forms of DR, glaucoma and AMD are usually not noticed by the patient, causing substantial damage unless diagnosed early [2].

DR is a complication in the retina due to diabetics. Its characteristic features are Microaneurysms (MA), Hemorrhages (H), and Exudates (hard exudates (HE) and soft exudates (SEx)). MA are discrete localized distension of the weakened capillary walls and are presented as small, circular

red ‘dots’ on the retina. In time, when the small blood vessels are ruptured, hemorrhages will be occurred. They generally appear either as a red ‘dot’ or ‘flame-shaped’ on the retina. HEs are caused by proteins and lipids leaking from the blood into the retina via damaged blood vessels. These appear in retinal images as yellow white areas, sometimes in a ring-like structure around leaking capillaries. When the severity of DR advances the blood vessels become obstructed which causes microinfarcts in the retina which are called SEx. If advanced, it results in diabetic macular edema (DME) [3]. AMD often affects the area of central vision (Macula). This is due to the process which is known as neovascularization that involves the growth of abnormal, leaking blood vessels under the macula, ending with atrophy and scarring of the macula. Glaucoma is an optic neuropathy, involving gradual damage to the retinal ganglion cells and their axons that lead into the optic nerve and further into the visual areas of the brain. The OD is pale red with a yellowish tint in the center of the retina. In the case of glaucoma the disc will have sharply denned borders and a shallow physiological cup [1, 3].

In clinical ophthalmology the examination of the optic fundus is important for determining the health of the fundus (posterior pole of the eye that includes the retina, macula, fovea, optic nerve, OD, blood vessels and other interior structures). It enables early detection and diagnosis of eye diseases due to DR, AMD and glaucoma. Various ophthalmoscope techniques such as digital fundus photography, indirect ophthalmoscopy, stereo bio-microscopy, fluorescein angiography, and optical coherence tomography (OCT) are used in diagnosis and management of eye diseases [3]. However because of its relatively low cost, simplicity and easy access fundus camera is used most of the time. It is satisfactory for viewing the fundus and the structures leading to it by 2-D representation of the 3-D retinal semi-transparent tissues (see Fig. 1.1). Most of the time it is used to detect and evaluate symptoms of retinal detachment or eye diseases due to DR.

Additionally it is used to record color images of the fundus in order to document the presence of disorders and monitor their change over time.

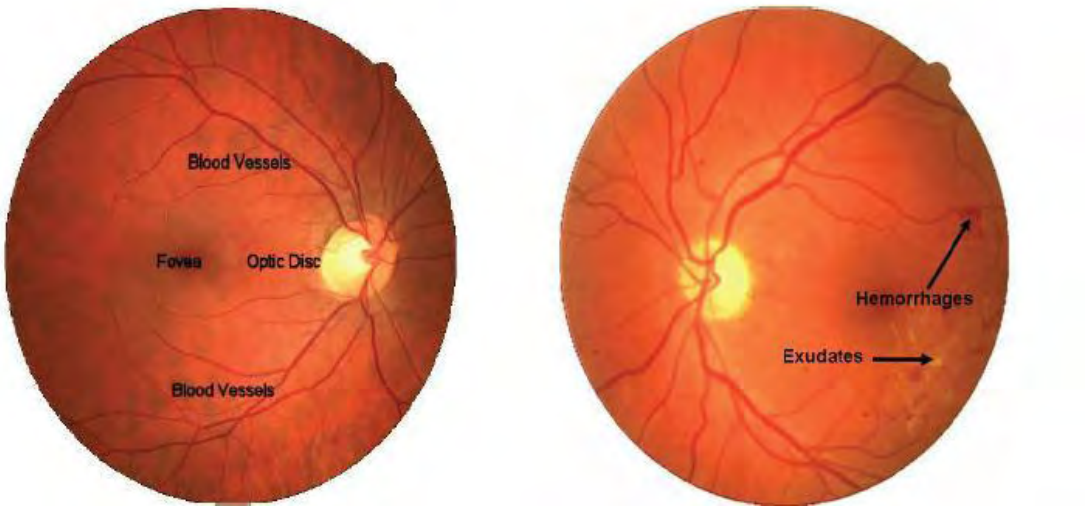

Figure 1.1: Typical structures of a color fundus image.

1.2. Statement of the problem

Accurate segmentation of fundus images is critical for mass screening and monitoring of ocular diseases. It provides a better source of information for studying the various ocular morphologies which is helpful to improve clinical outcomes, prognosis, patient diagnosis and treatment planning. However, manual segmentation is often a time-consuming and subjective process. Additionally, the retinal images acquired using low cost fundus camera are prone to various artifacts such as noise, poor image contrast, presence of anatomical structures with highly correlated pixels with that of lesion, illumination variability, color variation of similar subjects due to difference in background, size and shape variation of lesions, and movement of the eye during image acquisition. With increasing image data becoming available to ophthalmologists, the need and potential impact of image analysis methods is very high.

Recent advances in digital imaging and computing power have made it possible to use data provided from medical images in new and revolutionary ways. Such a system should be able to distinguish between affected and normal retinal images. The automatic diagnosis systems relieve physicians of repetitive work, increase efficiency and provide remarkable cost savings. The success of this type of screening approach depends on accurate fundus image capture, and especially on accurate and reliable image processing algorithms for detecting the abnormalities.

The focus of this thesis is especially on Exudates (EXs) detection and their differentiation from other bright areas, specifically cotton wools (CWs) and the OD which have similar features in color and brightness with HEs. As EXs are among common early clinical signs of DR, their detection would be an important asset to the mass screening tasks and could serve as a first step towards a complete monitoring and grading of the disease.

Several methods have been developed in the literature by many researchers for use in segmentation of HEs, blood vessels, fovea, and OD in fundus images. Some researchers attempted to detect EXs using their high luminosity to separate them from the background by tresholding [5-7]. The wide variability among images made the method dependent on user intervention to select the appropriate threshold for each case. In addition, since the attributes of OD are similar to attributes of HE in terms of color and brightness, such methods generate large number of false positives which result in their low percentage specificities when applied on large data sets. Most attempts try to detect features in fundus images using only one channel, usually the green channel [4, 5]. However those analysis techniques miss out color information that is present in the remaining channels. Other studies used edge detectors combined with morphological operations [8-11]. First, the borders of candidate EXs were detected. Then color, shape and location properties were used to separate true lesions. Other researchers focused on the

study of the ability of Bayesian classifiers to detect retinal lesions associated with DR [12, 13]. A statistical classifier together with Fisher's linear discriminant analysis (LDA) has also been used previously to segment EXs [14]. A method for detecting EXs and CWs, and separate them from drusen has also been proposed [15]. In this method a K-Nearest Neighborhood (KNN) classifier was used at the first stage to detect candidate bright lesions. LDA was subsequently used to differentiate among lesion types. In other study neural network (NN) based classifiers have been used [16-18]. A multilayer perceptron (MLP) was used in [16] to determine the presence of bright lesions. In [17] candidate bright regions were segmented using Fuzzy C-means clustering. A support vector machine (SVM) was used afterwards to determine if a segmented region is an EX or another type of bright region. A similar approach was used in [18], where multilayer perceptron NNs and SVM were analyzed and compared.

Generally, most attempts in fundus color image processing focus on analyzing each separate color components serially and combining the outputs from the different channels. However, such a serial method masks any existing inter-correlations between the color channels and the associated computational cost is often high. In this regard, a more holistic representation and analysis approach should have tremendous advantages. Recent application of higher dimensional algebra in color image analysis uses vectorial representations of the three color components in quaternion and trinion spaces and the respective integral transforms permit the analysis as one entity/object keeping the inter correlation information [19, 20]. Based on such a vectorial principle, a holistic and automated image processing scheme is suggested in this thesis to extract robust and relevant textural features for major abnormality markers in fundus images. The efficacy of image based higher order features in enhancing major abnormality markers and their

effectiveness in attenuating intra and inter image variations due to unwanted artifacts is thoroughly investigated.

1.3. Objectives

- **General objective:**
  - ✓ To come up with automated retinal color image processing method based on fundus camera that enables mass screening of ocular diseases in an effective way.

- **Specific objectives:**
  - ✓ To develop a holistic scheme for use in color retinal image analysis.
  - ✓ To extract robust and non redundant textural features.
  - ✓ To generate signature maps for use in enhancement of EXs and the OD.
  - ✓ Identification of abnormal retinal images and detection of major abnormality markers in the retina.

1.4. Significance of the study

The growing incidence of diabetes increases the number of images that need to be reviewed by physicians. In addition, the high cost of examinations and the lack of specialists prevent many patients from receiving effective treatment. Computer aided detection of retinal lesions associated with DR offers many potential benefits. In a screening setting, it allows the examination of a large number of images in less time and more objectively than current observer driven techniques. In a clinical setting, it can be an important diagnostic aid and can reduce the workload of trained graders, and, thereby reducing costs. Moreover, it is important to distinguish among lesion types as they have different diagnostic importance and management implications. The work in this study is comprised of robust image analysis algorithm development with

potentially useful pre-clinical and clinical applications which could contribute a lot to the existed problems.

1.5. Organization of the thesis

The thesis is organized in to six chapters. Chapter 2 provides background information, including a discussion of human eye structure and the characteristic features of normal and abnormal structures in the retina. Chapter 3 discusses the basic concepts of medical image processing techniques with their related applications. It also provides general background information, including detail discussions on the different types of image processing tasks and analysis techniques like feature extraction, texture analysis, image segmentation and classification techniques, and spectral analysis of color images. A review of algorithms that have been used by different researchers in the field for automatic segmentation of EXs, OD, and blood vessels is also included in this chapter.

Chapter 4 discusses the proposed retinal image processing methods and the data set that have been used in the current study. This includes selection of an optimal color space, a holistic representation and analysis of the resulting color images, and ways of extracting meaningful higher order statistical features for use in uniquely quantifying useful objects like HEs and the OD against the background. Additionally the soft segmentation scheme that has been used for automatic segmentation of HEs and classification of abnormal images due to DR is also discussed in this chapter. Chapter 5 discusses the results obtained from the methods in chapter 4. Quantitative and qualitative analysis techniques are held on the results to evaluate the performance of the proposed system. Finally, chapter 6 presents concluding remarks and possible future directions of the study.

References

1. M. A. Mir, Atlas of clinical diagnosis, Edinburgh, London, 2nd Ed., 2003.
2. M. K. Garvin, Automated 3-D segmentation and analysis of retinal optical coherence tomography images, PhD Dissertation, University of Iowa, Iowa City, USA, 2008.
3. K. M. Kade, Fundus Image Acquisition Techniques with Data base in Diabetic Retinopathy, IJERA, 3(2), pp. 1350-1362, 2013.
4. N. P. Ward, S. Tomlinson, and C. J. Taylor, Image analysis of fundus photographs - The detection and measurement of exudates associated with diabetic retinopathy, Ophthalmology, 96(1), pp. 80-86, 1989.
5. R. Phillips, J. Forrester, and P. Sharp, Automated detection and quantification of retinal exudates, Graefes Arch. Clin. Exp. Ophthalmol. 231(2), pp. 90-94, 1993.
6. D. Kavitha and S. S. Devi, Automatic detection of optic disk and exudates in retinal images, Proc. Int. Conf. Intelligent Sensing and Information Processing, pp. 501-506, 2005.
7. Z. Liu, O. Chutatape, and S. M. Krishnan, Automatic image analysis of fundus photographs, IEEE Eng. Medicine Biol. Soc., Chicago, USA, Vol. 2, pp. 524-525, 1997.
8. K. Akita and H. Kuga, A computer method of understanding ocular fundus images, Pattern Recogn., 15(2), pp. 431-443, 1982.
9. H. Li and O. Chutatape, Fundus image features extraction, IEEE Eng. Med. Biol. Soc., Chicago, USA, 19(1), pp. 3071-3073, 2000.
10. H. Li and O. Chutatape, Automated feature extraction in color retinal images by a model based approach, IEEE Trans. Biomed. Eng., 51 (4), pp. 246–254, 2004.
11. G. Zahlman, B. Kochner, I. Ugi, D. Schuhmann, B. Lisenfeld, A. Wegner, M. Obermaier, and M. Mertz, Hybrid fuzzy image processing for situation assessment: A knowledge-based system for early detection of diabetic retinopathy, IEEE Eng. Med. Biol. Mag., 19 (2), pp. 76-83, 2000.
12. H. Wang, W. Hsu, K. G. Goh, and M. L. Lee, An effective approach to detect lesions in color retinal images, IEEE Computer Society Conference on Computer Vision and Pattern Recognition, Hilton Head Island, SC, USA, pp. 181-186, 2000.
13. B. M. Ege, O. K. Hejlesen, O. V. Larsen, K. Moller, B. Jennings, D. Kerr, and D. A. Cavan, Screening for diabetic retinopathy using computer based image analysis and statistical classification, Comput. Methods Programs Biomed., Vol. 63, pp. 165-175, 2000.

14. C. I. Sanchez, R. Hornero, M. I. Lopez, C. M. Aboy, C. Poza, and D. Abasolo, A novel automatic image processing algorithm for detection of hard exudates based on retinal image analysis, Medical Engineering & Physics, Vol. 30, pp. 350 -357, 2008.
15. M. Niemeijer, B V. Ginneken, S. R. Russell, M. A. SuttorpSchulten, and M. Abromoff, Automated detection and differentiation of drusen, exudates, and cotton-wool spots in digital color fundus photographs for diabetic retinopathy diagnosis, Invest. Ophthalmol. Vis. Sci., Vol. 48, pp. 2260-2267, 2007.
16. G. G. Gardner, D. Keating, and T. H. Williamson, A. T. Elliot, Automatic detection of diabetic retinopathy using an artificial neural network: a screening tool, British J. Ophthalmol. Vol. 80, pp. 940–944, 1996.
17. X. Zhang and O. Chutatape, Top-down and bottom-up strategies in lesion detection of background diabetic retinopathy, IEEE Computer Society Conference on Computer Vision and Pattern Recognition, San Diego, USA, pp. 181-186, 2005.
18. A. Osareh, Automated identification of diabetic retinal exudates and the optic disc, PhD Dissertation, Bristol, 2004.
19. D. Assefa, L. Mansinha, K. F. Tiampo, H. Rasmussen, and K. Abdella, Local quaternion Fourier transform and color image texture analysis, Sig Proc., 90(6), pp. 1825-1835, 2010.
20. D. Assefa, L. Mansinha, K. F. Tiampo, H. Rasmussen, and K. Abdella, The trinion Fourier transform of color images, Sig Proc., 91(8), pp. 1887-1900, 2011.

Chapter Two

2. The human eye and retinal diseases

2.1. Overview of the structure and functionality of the eye

When rays of light enter the eye, they are focused onto the retina by the cornea, pupil and the lens. The nerve impulses produced by the retina are sent along the optic nerve to the brain to interpret the image that we see. The eye consists of many complicated parts, including supportive layers, optical components and neural components. Fig. 2.1 shows the 3D schematic illustration of the human eye with its constituent parts. The eyeball is coated by sclera, which is a white, dense, fibrous layer. The cornea is a transparent layer of the eyeball which covers the iris and pupil. In addition the cornea provides two-third of the refractive power of the eye. The light rays pass to the lens through the pupil, which is an opening in the centre of the iris. The iris is the colored diaphragm in the anterior chamber of the eyeball which contracts and expands to control light intensity. The lens is a dual-convex clear crystalline organ which focuses light rays onto the retina. The posterior chamber of the eyeball is filled with a clear jellylike substance called vitreous fluid, and is normally attached to the retina. The retina is the membrane on the inner wall of the eyeball divided into two developmental layers, the pigment layer and the neural layer which receives the rays of light from the lens and converts it into nerve impulses. These impulses travel along the optic nerve to the brain, where they are converted to images. There are two types of photoreceptors contained in the retina: rods and cones. With their central location, cones are responsible for bright light and colors, while the rods are responsible for peripheral and night vision. The macula refers to the important centre of the retina which is responsible for central vision. The fovea is the central area of the macula which is responsible for sharp vision and is

the region of highest visual acuity and cone cell density. The OD is the area where the optic nerve is connected to the retina and can be seen as a bright yellow disc. All of the blood vessels supplying the retina enter and exit via the OD. Its diameter is often used as a standard to measure distances and sizes in the fundus image [1].

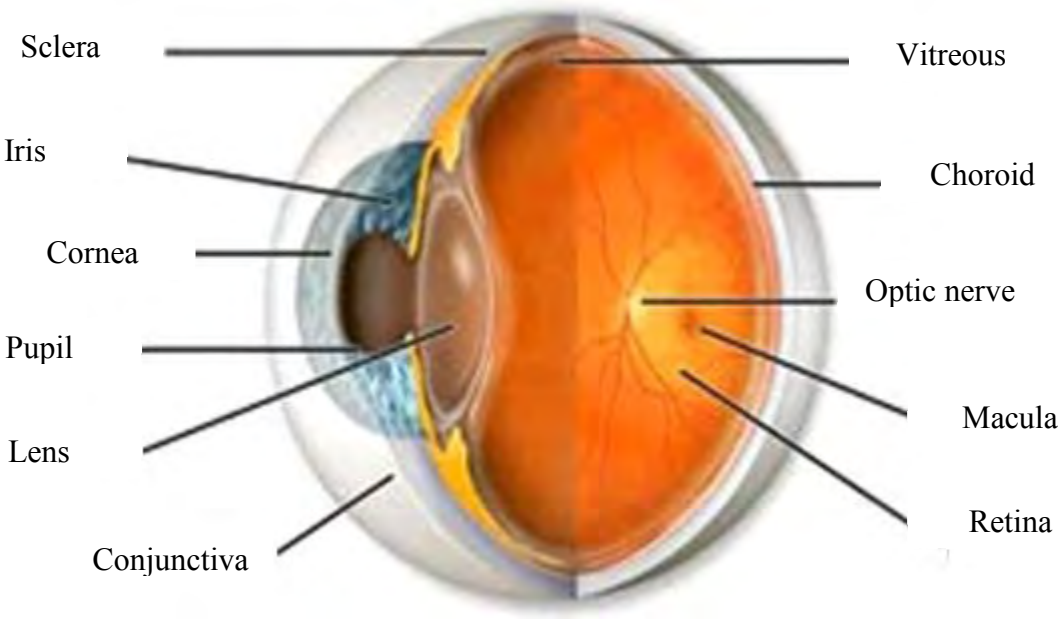

Figure 2.1: 3D illustration of the human eye. Courtesy of Mir et al.

2.2. Characteristic features of normal and abnormal structures in color fundus images

Fundus eye mainly refers to the posterior pole of the eyeball, especially the retina, the macula, OD, optic nerve and other interior structures of the eye [2]. Fig. 2.2 shows a sample color retinal image, which is acquired with digital fundus camera, with major anatomical structures. Fundus image test enables detection of eye diseases based on characteristic features of major anatomical

and pathological structures of the retina. It can also detect diseases not linked directly to the eye, such as systemic nerve disorder and hypertension.

The most common ophthalmic devices for non-invasive examination of fundus eye are the ophthalmoscope and the fundus camera, which are very useful for a first diagnosis as well as monitoring of retinal pathologies. But these devices provide flat images, and do not provide information about the topography of the fundus eye. Other more sophisticated equipments allow high resolution and contrast reconstructions. However, these devices have a high cost and the resulting images are monochromatic [2].

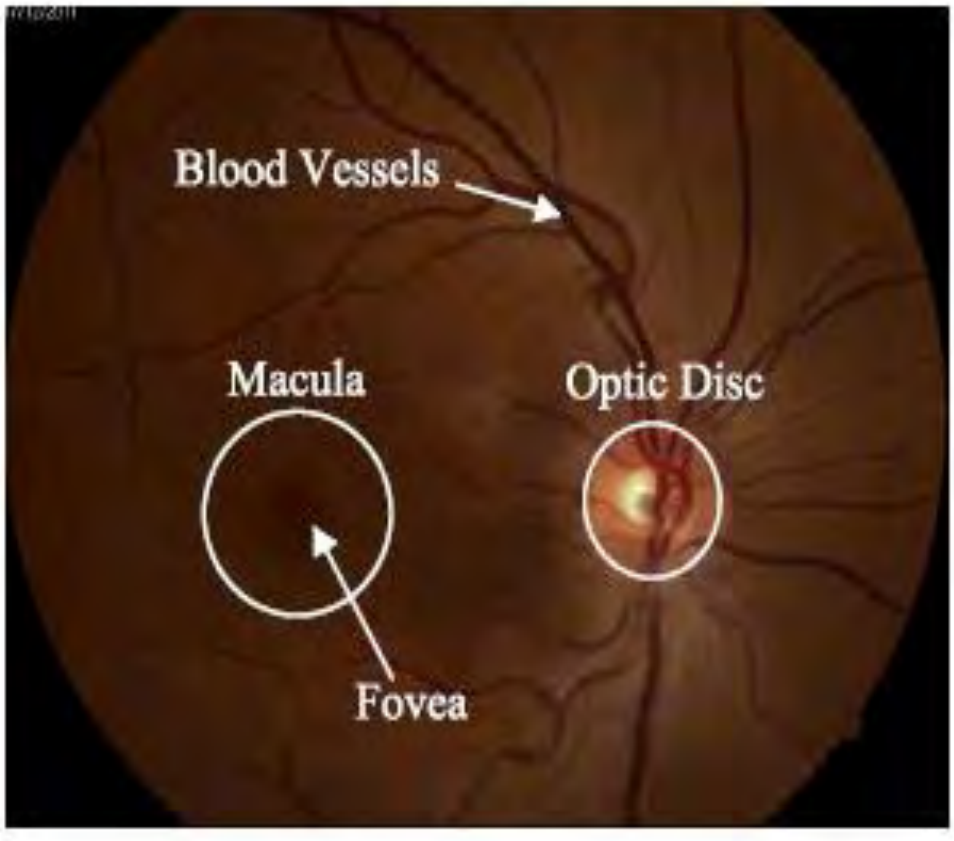

Figure 2.2: Color retinal fundus image with main anatomical structures

2.2.1. The normal fundus

The major normal structures in the fundus are OD, blood vessels, macula and fovea. In color fundus image those structures can be identified and differentiated based on their color, shape and textures. However, owing to the combined color of the pigmented epithelium and the underlying vessels, the color of a normal fundus varies from subject to subject. In general the color of a normal Caucasian fundus varies from orange to vermilion, that of a dark Asian person may be yellowish-grey or coffee-brown, and that of an African subject tends to be chocolate-brown.

The OD is pale red with a yellowish tint. It is usually circular or vertically oval. The relative pallor of the disc is largely the result of the reflection of light from the myelin sheaths of the optic nerve. In most normal fundus the disc has a funnel-shaped depression (known as physiological cupping) at its centre from which the retinal vessels seem to emerge. The macula lies at approximately 1-1.5 disc widths from the temporal border of the OD. It is a horizontally oval depression recognizable by the contrast of its red color with that of the paler surrounding fundus. At the centre of the macula lies a smaller depression called the fovea. This is a very thin part of the retina and allows the brighter red color of the underlying choroidal circulation to shine through. This is the normal fovea reflex. Retinal blood vessels appear as dark red color. They form four groups to supply the four quadrants of the fundus. These four principal divisions of the retinal vessels follow a sinuous course and divide dichotomously as they proceed to their respective quadrants. From the superior and inferior temporal vessels, small branches pass towards the macula where they terminate in fine twigs around the margin of the macular depression. They stop short of the vascular fovea, which gets its red color, and oxygen, from the underlying choroidal vessels. The ophthalmoscopy white axial reflex, which runs along the centre of each vessel, is caused by the surface of the blood column and the vessel wall [1].

2.2.2. Abnormities in fundus

Major abnormalities (pathological structures) in the retina appear due to eye diseases such as DR and glaucoma. DR is a micro vascular complication of diabetes, causing abnormalities in the retina, and in the worst case, blindness. The main characteristic features of DR are MA, EXs (HEs and SEx), hemorrhages, and DME. EXs are the major prevalent lesions during the early stages of DR. In fundus image they generally appear as yellow white areas.

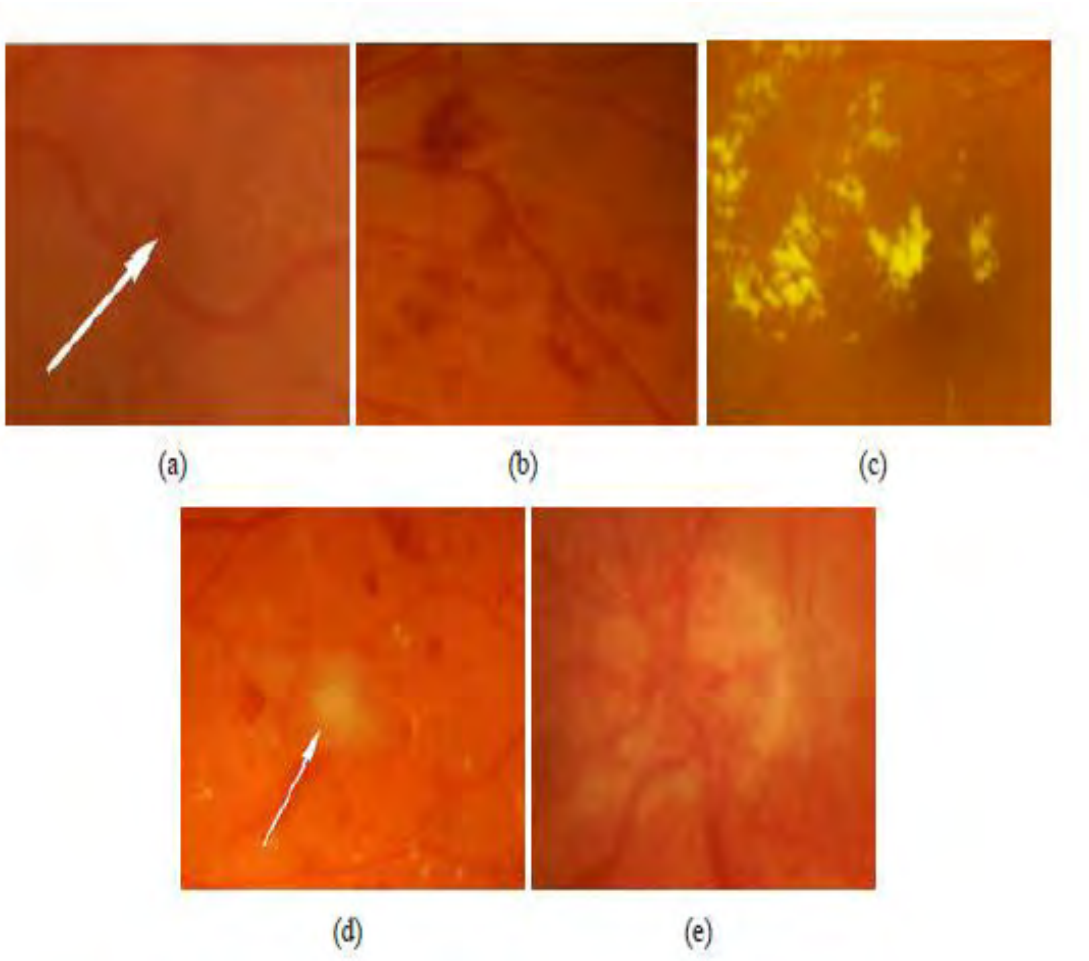

Figure 2.3: Abnormal findings in the eye fundus caused by diabetic retinopathy: (a) Microaneurysms (marked with an arrow), (b) hemorrhages, (c) hard exudates, (d) soft exudates (marked with an arrow), and (e) neovascularization. Courtesy of Kauppi et al.

Typically there are no salient symptoms in the early stages of DR, but the number and severity predominantly increase through time. DR typically begins as small changes in the retinal capillaries. The first detectable abnormalities are MAs which are local distensions of the retinal capillaries and appear as small red dots [3] as shown in Fig. 2.3a. Most of the time it is difficult to distinguish MAs in fundus images due to their small sizes. MAs cause intraretinal hemorrhage when it is ruptured. Hemorrhage appears as flame shaped red dot in the fundus image as shown in Fig. 2.3b. The disease severity is classified as mild non-proliferative DR when the first apparent MA appears in the retina. In time, the retinal edema and HEs are followed by the increased permeability of the capillary walls. HEs are lipid formations leaking from these weakened blood vessels. It leads to swelling of the macular tissue and damage to photoreceptors. It appears as yellow white areas, sometimes in a ring-like structure around leaking capillaries (Fig. 2.3c). This state of the retinopathy is called moderate non-proliferative DR. However, if the above-mentioned abnormalities appear in the central vision area (macula), it is called diabetic maculopathy [2, 4, 5]. As the retinopathy advances, the blood vessels become obstructed which causes microinfarcts in the retina. These microinfarcts are called soft exudates (SEx) and appear as pale yellow area (Fig. 2.3d). When a significant number of intraretinal hemorrhages, SEx, or intraretinal micro vascular abnormalities are encountered, the state of the retinopathy is defined as severe non proliferative DR. The severe non proliferative DR can quickly turn into proliferative DR when extensive lack of oxygen causes the development of new fragile vessels [4, 5]. This is called neovascularization which is a serious eye sight threatening state [4]. It involves the growth of abnormal, leaking blood vessels under the macula, ending with atrophy and scarring of the macula (Fig. 2.3e). The proliferative DR may cause sudden loss in visual acuity or even a permanent blindness due to vitreous hemorrhage or fractional detachment of the

central retina. After diagnosis of DR, regular monitoring is needed due to the progressive nature of the disease. However, broad screenings cannot be performed due to the fact that the fundus image examination requires attention. For an effective mass screening, automatic image processing methods must be developed [6, 7].

Glaucoma is an optic neuropathy, involving gradual damage to the retinal ganglion cells and their axons that lead into the optic nerve and further into the visual areas of the brain. The shape, width and depth of the physiological cup, the margin and the color of the disc, together with the state of the vessels, should all be scrutinized carefully for evidence of glaucomatous disease. In simple, or primary, optic atrophy (from injury, ischemia or toxic damage to the optic nerve) the disc is pale with sharply denned borders and a shallow physiological cup (Fig. 2.4a). Sometimes the pallor is not very striking unless a comparison is made with a normal fundus. In advanced cases, there is marked narrowing of the retinal vessels. In glaucomatous optic atrophy, the cup is enlarged and occupies a larger part of the disc. Its margin shows an abrupt step down from the retinal level and the emerging vessels appear to bend sharply outwards (see Fig. 2.4b, for example). Papilloedema, or a non inflammatory edema of the optic nerve head, is an important diagnostic sign of many systemic, intracranial and orbital disorders. The earliest changes are a blurring of the disc margin, hyperemia and swelling of the papilla (OD) (Fig. 2.4.c). These changes start at the periphery of the disc leaving the central cup well-preserved until late on in the disease. As the intracranial pressure remains elevated, the cup fills up, the disc becomes hyperemic with dilated capillaries and the margin becomes completely obliterated (see Fig. 2.4.d). There is venous dilatation and the surrounding retina becomes involved with the appearance of soft, white patches. At this stage, clinical examination often reveals enlargement of the blind spot (Fig. 2.4.e). In chronic glaucoma the funnel in the optic cup is deep

(glaucomatous cupping) and the emerging vessels appear to bend sharply at its edge (Fig. 2.4.f) [1].

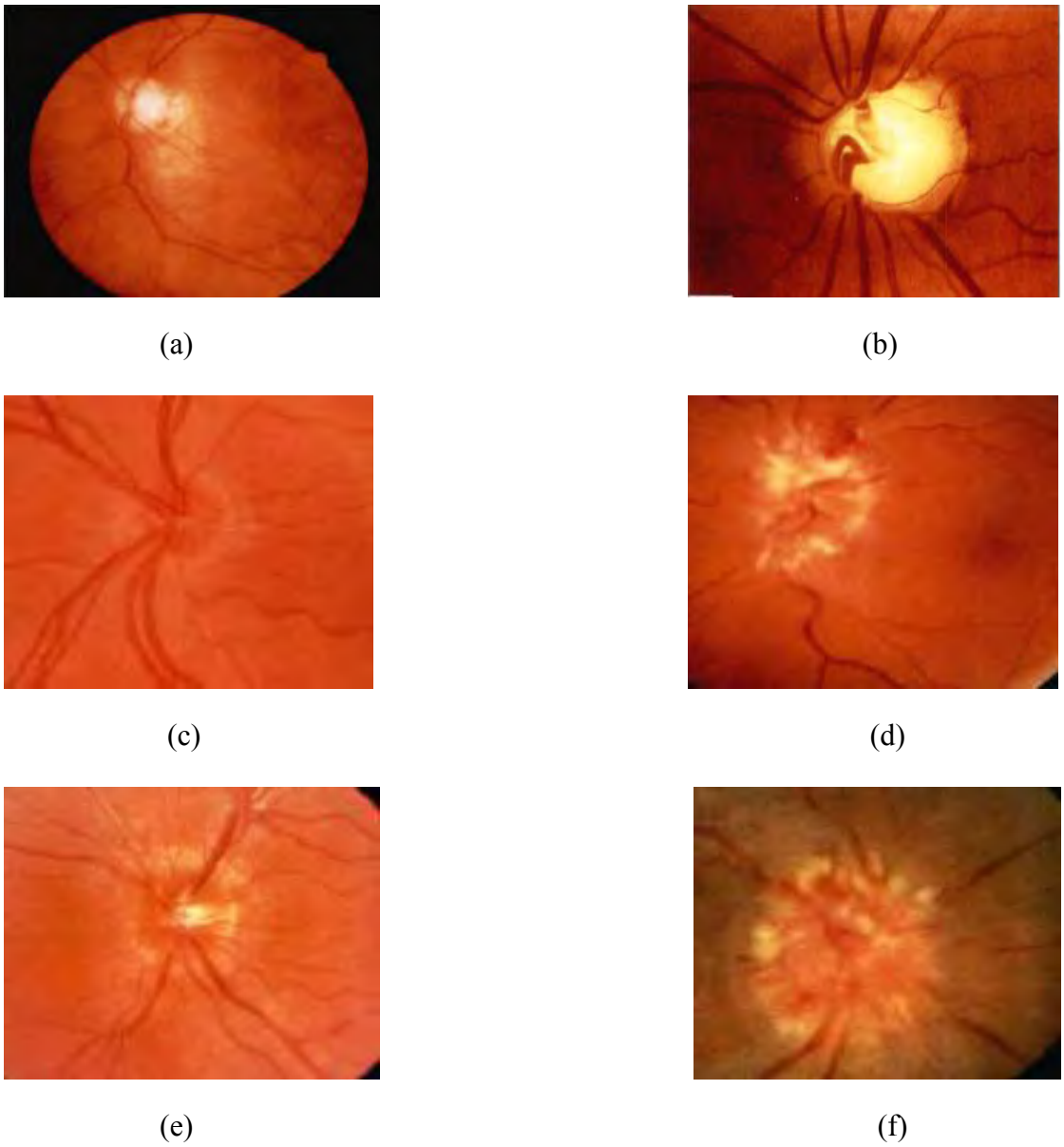

(a) (b)

(c) (d)

(e) (f)

Figure 2.4: Abnormal findings in the eye fundus caused by glaucoma: (a) Optic atrophy with pale disc and attenuated vessels, (b) Glaucomatous optic atrophy: sharply angulated vessels and pale disc, (c) Papilloedema: swollen, hyperemic disc with blurred margins, (d) The pale central core of the disc surrounded by hyperemia, (e) Advanced Papilloedema with congestion and edema of the disc, (f) Advanced papilla edema: tortuous and congested veins with edema. Courtesy of Mir et al.

References

1. M. A. Mir, Atlas of clinical diagnosis, Edinburgh, London, 2nd edition, 2003.
2. K. M. Kade, Fundus Image Acquisition Techniques with Data base in Diabetic Retinopathy, IJERA, 3(2), pp. 1350-1362, 2013.
3. J. J. Kanski, Clinical Ophthalmology: A Systematic Approach, ISBN, pp. 5542-5549, 2003.
4. L. B. Backlund, Early Diagnosis of Diabetic Retinopathy by Mass Examinations in Primary Health Care, PhD dissertation, Karolinska Institute, Sweden, 2000.
5. D. E. Singer, D. M. Nathan, H. A. Fogel, and A. P. Schachat, Screening for diabetic retinopathy, Annals. of Int. Medicine, Vol. 116, pp. 660-671, 1992.
6. T. Kauppi, V. Kalesnykiene, J. Kamarainen, L. Lensu, I. Sorri, A. Raninen, R. Voutilainen, H. Uusitalo, H. Kalviainen and J. Pieti, DIARETDB1: diabetic retinopathy database and evaluation protocol, pp. 1-18, 2010.
7. T. Kauppi, V. Kalesnykiene, J. Kamarainen, L. Lensu, I. Sorri, H. Uusitalo, H. Kalviainen, and J. Pieti, DIARETDB0: Evaluation Database and Methodology for Diabetic Retinopathy, pp. 1-17, 2008.

Chapter three

3. Medical image processing and applications

3.1. Image processing

Image processing can be defined as the manipulation of an image either to enhance visual appearance or to prepare images for quantitative measurement of features for object recognition. This thesis concentrates on both. Main interest in digital image processing methods stems from two principal application areas: improvement of pictorial information for human interpretation; and processing of image data for storage, transmission, and representation for autonomous machine perception [1]. There are numerous specific motivations for image processing but many fall into the following categories: (i) to remove unwanted signal components that are corrupting the image and (ii) to extract information by rendering it in a more obvious or more useful form. The principal objective of enhancement is to process an image so that the result is more suitable than the original image for a specific application. However, image processing is very much problem oriented task. For instance a method that is quite useful for enhancing fundus images may not necessarily be the best approach for enhancing MR or X-ray images.

3.1.1. Computer vision and human vision

Computer vision and human vision appear to have the same function and goal [2]. Both systems interpret multidimensional spatial data for the purpose of information gathering and visual recognition. Due to the complexity of the human visual system and the lack of total understanding of the neural aspects of human perception, even the best computer vision system cannot replicate the human eye. The development of image processing technique is then focused on improving upon the human vision model rather than replicating it. Vision is the ability to

focus selectively on objects of interest. The human eye can discern thousands of color shades and about two-dozen shades of gray. Human vision is a complex system that senses and acts on visual stimuli in the form of light. For instance, as it is demonstrated in [2], the human brain compensates for loss of acuity by emphasizing boundaries between regions of differing intensities. The demonstration shown in Fig. 3.1a, which is often termed Mach band, consists of several stripes represented by constant intensity in increasing order. Although each stripe is of a constant intensity, in the borders they appear to change slightly from light to dark. In other words, there appears a faint lighter border to one side and a faint darker border to the other side of each of the internal boundaries. The gradation within each stripe does not exist, but rather is perceived by the human eye. Fig. 3.1b shows the actual intensity levels while Fig. 3.1c illustrates the perceived intensity values. The visual perception of Mach bands at boundaries between intensity levels is thought to assist in the discernment of boundaries to make up for decreased visual acuity. This phenomenon is particularly important in the field of medical diagnosis, as a gradient in intensity may appear in an image where the image data does not support this observation.

Human vision, which is augmented by a brain that has been specialized to ensure the survival of humankind, may present different perceptions and images than computer vision, which depends upon an algorithm designed for the processing of discrete pixel information contained in image data. The use of experts, or the human eye, makes for subjective grading criteria where inferences are based on experience which may include information not actually present in the image data. This may be an advantage or disadvantage depending on the experts and their domain knowledge. In any case, augmenting subjective information with quantitative data from

the diagnostic imaging provides the expert with objective information for arriving at a diagnostic conclusion.

(a)

(b) (c)

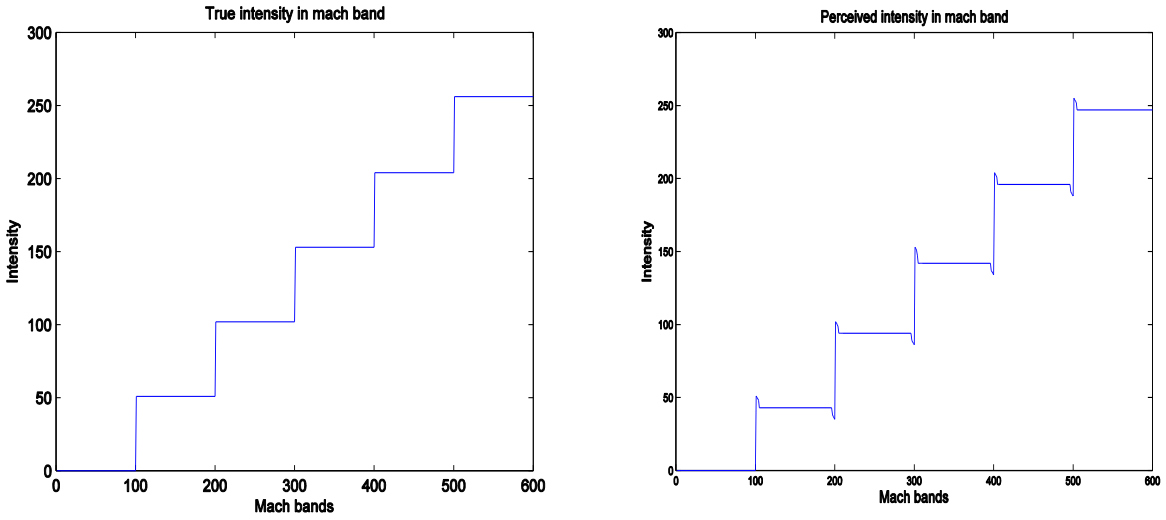

Figure 3.1: Mach band example, (a) Mach band, (b) true intensity profile in mach band, and (c) perceived intensity in mach band.

3.1.2. Image data structure

Digital images are comprised of a set of points or picture elements, usually referred to as pixels, stored as an array of numbers. They are spatial data indexed by two spatial coordinates; typically

the variables x and y refer to the horizontal and vertical axes of an image. Pixel value represents the color or intensity of each pixel, and the placement of the pixels within the matrix corresponds to their placement within the image. If more than one value is required to encode pixel information, the image is often represented by a multidimensional matrix. For example, an RGB encoding of an image would contain 3 matrices: one each for red, green and blue intensities. In other terms, each pixel represented in the matrix has a value that is encoded as either a scalar (in the case of gray-scale) or a vector (in the case of color).

- **Color spaces:**

Color is the way the human visual system measures a part of the electromagnetic spectrum, approximately between 400 and 650nm [3]. Because of certain properties of the human visual system we are not able to see all of the possible combinations of the visible spectrum but we tend to group various spectra into colors.

A color space is a notation by which we can specify colors, i.e. the human perception of the visible electromagnetic spectrum. Because manipulation of colors is possible through additive properties (for example, red and green produce yellow) a wide range of colors is generated from a choice of the three primary colors. A red, blue and green (RGB) color space is commonly used in modern displays like televisions, computer monitors and digital cameras [2, 3]. Each primary color has a range of values dependent on bit resolution. Most digital systems store color channels in 8-bit quantities, allowing a range from 0 to 255 to indicate the intensity of a color. This is referred to as 24-bit RGB or true color and allows for 16,777,216 (256^3) different colors. In the cases of white, black and shades of gray, white is represented by maximum intensity over all three channels, black is represented by nil intensity over all three channels and shades of gray are represented by equal intensities over all three channels.

The RGB color space is represented via a three-dimensional cube as shown in Fig. 3.2. The coordinates of each point inside the cube represent the values of each primary color. There are three laws of colorimetry (which deals about the determination of a color and its constituents): first, the creation of any color is possible with the three primary colors and any given combination of the primary colors is unique; second, any two colors which are equivalent are again equivalent after multiplying or dividing all three components by a scalar; and third, the luminance of a mixture of colors is equal to the sum of the luminances of each color component [3, 4].

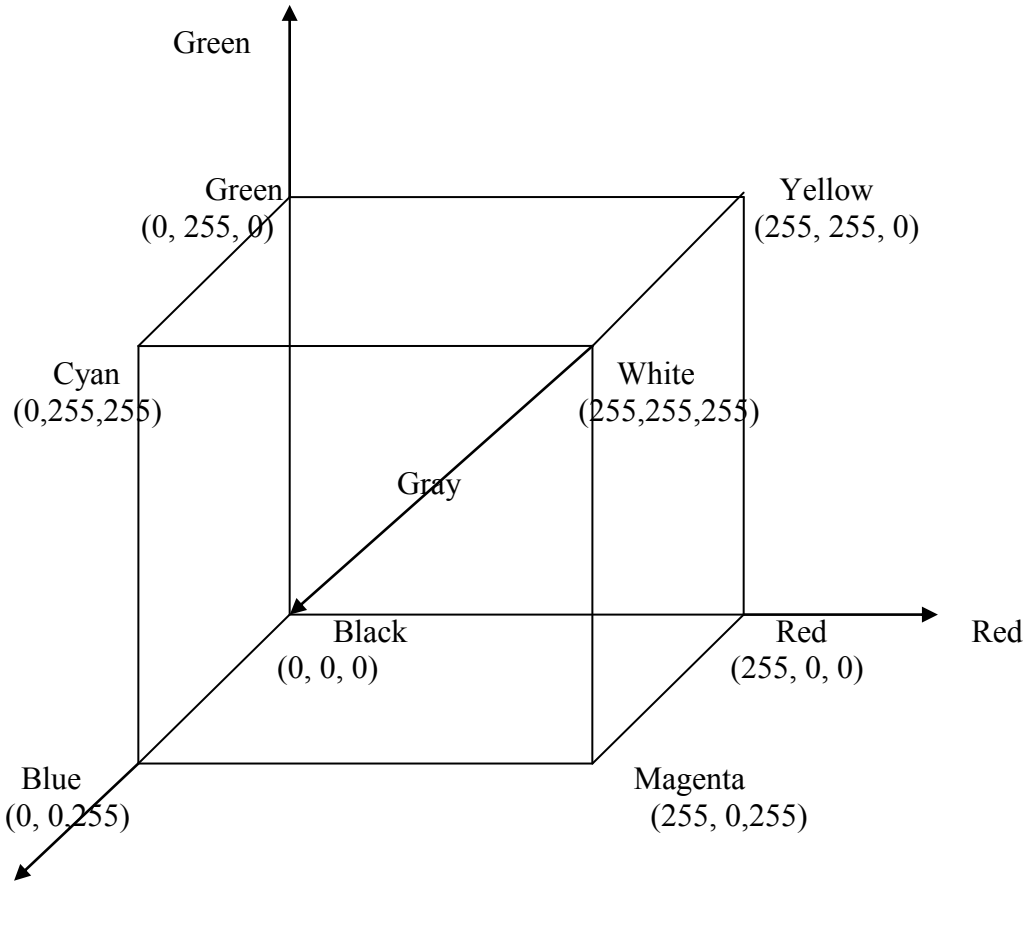

Figure 3.2: RGB color space represented by a cube

There are also other color spaces such as Lab, CMYK, HSV, LUV, YCrbCrr, CIE L*a*b, and CIE L*u*v which might be more useful in applications than just RGB. Since color space selection is application dependent, transforming images from RGB to a desired space for the specific problem is very beneficial [4]. The choice of the color space can be a very important decision which can dramatically influence the results of image processing. The knowledge of various color spaces can ease the choice of the appropriate color space.

Although there is no agreement on which color space is the best for image processing applications and content based image retrieval (CBIR), an appropriate color system is required to ensure perceptual uniformity [5]. Therefore, the RGB color space, a widely used system for representing color images, is not suitable for CBIR because it is a perceptually non-uniform and device-dependent system [6]. The most frequently used technique is to convert color representations from the RGB color space to the HSV, CIE L*u*v, or CIE L*a*b color spaces for perceptual uniformity [7]. The HSV color space is an intuitive system, which describes a specific color by its hue (H), saturation (S), and brightness (V). The brightness is also referred as the value or luminosity. This color system is very useful in interactive color selection and manipulation. The CIE *L*u*v* and CIE *L*a*b* color spaces are both perceptually uniform systems, which provide easy use of similar metrics for comparing colors [7]. Colors like the CMYK are commonly used for printing and not that much in image processing.

After selecting a color space, an effective color descriptor should be developed in order to represent the color of the global or regional areas. Several color descriptors have been developed from various representation schemes, such as color histograms, color moments, color edge, color texture, and color correlograms [8-12]. For example, color histogram, which represents the distribution of the number of pixels for each quantized color bin, is an effective representation of

the color content of an image. The color histogram not only easily characterizes the global and regional distribution of colors in an image, but also be invariant to rotation about the view axis.

For the retrieval of medical images, color allows images to reveal many pathological characteristics. Color also plays an important role in morphological diagnosis [13]. Color medical images are acquired using different imaging devices. For example, color endoscopic images are taken by a camera that is put into the hollow organs of the body such as stomachs and lungs. A common characteristic in such kinds of images is that most colors are made of various stains, though fine variations of natural colors are crucial for diagnosis. The ability to acquire color medical images, however, does not come without challenges. To mention few: inaccurate color reproduction, rough gradations of color, and insufficient density of pixels [13].

3.2. Basic image processing tasks and applications

3.2.1. Feature extraction

Feature extraction plays a vital role in various image processing tasks including object classification, pattern recognition and image segmentation. Features offer relevant information and descriptions of objects contained in a given subject. Hence, feature extraction methodologies basically analyze image attributes to extract the most prominent features that are representative of the various classes of objects. Features are used as inputs to classifiers that assign them to the class that they represent. The challenge is then how to identify which features are effective for representing the contents of the images and design of a robust scheme to carry out that kind of task. For instance, in brain tumor classification based on MR images, features if selected carefully are representative of the maximum relevant information that the image has to offer for a complete characterization of lesions [14, 15].

In image processing, feature extraction involves a special form of dimensionality reduction. When the input data to an algorithm is too large to be processed and it is suspected to be notoriously redundant (much data, but not much information) then the input data will be transformed into a reduced set of features (also named feature vector). Transforming the input data into the set of features is what we call feature extraction. If the features extracted are carefully chosen it is expected that the features set will extract the relevant information from the input data in order to perform the desired task using this reduced representation instead of the full size input [15]. Thus feature extraction involves simplifying the amount of resources required to describe a large set of data accurately. When performing analysis on complex data, one of the major problems stems from the number of variables involved. Analysis with a large number of variables generally requires a large amount of memory and computation power. Feature extraction is a general term for methods of constructing combinations of the variables to get around these problems while still describing the data with sufficient accuracy.

Various researchers proposed several combinations of feature vectors for image processing applications. Some of them are:

- Shape features such as circularity, irregularity, area, perimeter, shape index [2, 15, 16].
- Intensity features such as mean, variance, standard deviation, median, Skewness, and Kurtosis [14].
- Texture features such as contrast, correlation, entropy, energy, homogeneity, cluster shade, and cluster prominence [15, 16].
- Color features such as color histogram, color moments, color edge, color texture, and color correlograms [9-12].

The various features can further be classified as follows:

- General features: application independent features such as color, texture, and shape. According to the abstraction level, they can be further divided into:
    - ✓ Pixel-level features: features calculated at each pixel, e.g. color, location.
    - ✓ Local features: features calculated over the results of subdivision of the image band on image segmentation or edge detection.
    - ✓ Global features: features calculated over the entire image or just regular sub-area of an image.
- Domain-specific features: application dependent features such as human faces, fingerprints, and conceptual features. These features are often a synthesis of low-level features for a specific domain.

Feature selection

Feature selection is the technique of selecting a subset of relevant features for building robust learning models by removing most irrelevant and redundant features from the data. Feature selection helps to improve the performance of learning models by:

- Alleviating the effect of the curse of dimensionality.
- Enhancing generalization capability.
- Speeding up learning process.
- Improving model interpretability.

Feature selection also helps to acquire better understanding about a data through identifying most important features and their relations with each other.

Dimension reduction

In an attempt to capture useful contents of an image and to facilitate effective querying of an image database, a specific image processing system may extract a large number of features from

the content of an image. Feature set of high dimensionality causes the "curse of dimension" problem in which the complexity and computational cost of the query increase exponentially with the number of dimensions [17].

To reduce the dimensionality of a large feature set, the most widely used technique in image retrieval is principal component analysis (PCA). The goal of principal component analysis is to specify as much variance as possible with the smallest number of variables [18]. Principal component analysis involves transforming the original data into a new coordinate system with low dimension, thus creating a new set of data. The new coordinate system removes the redundant data, and the new set of data may better represent the essential information. However, there is a trade-off between the efficiency obtained through dimension reduction and the completeness of the information extracted. As data is represented with lower dimensions, the speed of retrieval is increased, but some important information may be lost in the process of data transformation.

Another dimensional reduction technique is Linear Discriminant Analysis (LDA). It is a supervised linear discriminator that uses the class information to find a set of vectors that maximizes the between-class scatter while minimizing the within-class scatter. Both PCA and LDA have shown useful applications in medical image analysis. For example, PCA has been used in areas of medical image retrieval for classifying brain MR images [19]. Retinal image analysis technique for EX detection has also been done based on LDA [20].

3.2.2. Texture analysis

Texture analysis occupies an important place in many advanced and sophisticated image processing tasks. Texture is an intuitive concept that describes properties like smoothness,

coarseness and regularity of a region [21]. Texture is an important element to human vision; it provides cues to scene depth and surface orientation. People also tend to relate texture elements of varying size to a plausible 3D surface. If images are represented in gray levels, texture becomes a crucial feature, which provides indications about scenic depth, the spatial distribution of tonal variations, and surface orientation [21]. In this sense a texture can be defined as a regional property which is characterized by the spatial distribution of gray levels in a neighborhood. For example, take abnormal symptoms on female breasts such as calcification, architectural distortion, asymmetry, and masses. All of those reveal specific textural patterns on the mammograms.

Texture analysis has been applied extensively in different image processing areas, ranging from geosciences and optical physics to various industrial applications. In medical imaging, texture analysis has been found very useful to enhance the available information. For example, in fundus imaging texture analysis has been applied for shape estimation of the OD. In brain imaging, texture analysis has been applied to various tasks such as tissue characterization and classification, and automatic image segmentation. In CBIR systems, texture has been one of the most important characteristic which has been used to classify and recognize objects and have been used in finding similarities between images in multimedia databases [5]. Texture, on its own does not have the capability of finding similar images, but it can be used to classify textured images from non-textured ones and then be combined with another visual attribute like color to make the retrieval more effective.

Visual analysis of texture is often a difficult task, especially in medical images where, in general, the texture patterns may be very subtle and their assessment very subjective. Additionally the basic pattern and repetition frequency of a texture sample could be perceptually invisible,

although quantitatively present. Quantitative texture analysis attempts to provide objective metrics. The analysis determines neighborhoods around pixels (texture elements) for which the voxel intensities and spatial relationship between them is used to extract certain quantitative features that characterize the texture of this neighborhood.

Analysis of texture requires the identification of proper attributes or features that differentiate the textures of the image. Basically, texture analysis approaches can be classified into statistical approaches and structural approaches. Statistical approaches analyze textural characteristics according to the statistical distribution of image intensity. Approaches in this category include gray level co-occurrence matrix (GLCM), fractal model, Tamura feature, Wold decomposition, and so on. Structural approaches characterize texture by identifying a set of structural primitives and certain placement rules. An example is description of texture based on regularly spaced parallel lines [5].

An image is basically comprised of one or several textures. Generally an image region has a constant texture if a set of its local properties in that region is constant, slowly changing or approximately periodic. Statistical approaches are widely employed in texture recognition and description of an image. Such methods include, for example, measurement of local image variations to help in contrasting image elements, calculation of auto correlation functions for an image based on spatial frequencies (either in spatial or frequency domains), calculation of correlations to measure image linearity and the like [22].

For grey scale image analysis there are lots of fairly good algorithms available to perform texture analysis. For color images, however, there is still enough challenge left to work on. In that regard, new algorithms for color texture analysis are increasingly being explored as color

analysis becomes feasible [23]. One of the approaches that have been proposed several times now is the so called color correlograms [11, 12, 23]. Alternative methods have also been proposed in the literature [24, 25], one of the most important being color histogram. The color histogram is extremely easy to compute and insensitive to small changes in viewing positions and partial occlusion. Due to the lack of any spatial information, however, the histogram is liable to false positives. Extensions of the color histogram are also investigated in [21]. It is the aim of this thesis to investigate a robust and reliable color texture analysis technique for use in classification, segmentation, and enhancement of retinal images.

3.2.3. Image segmentation and classification

There are three primary issues in texture analysis: classification, segmentation and shape recovery from texture. Image segmentation is a classification problem and therefore is one of the most important and difficult tasks in image processing. Classically, image segmentation is defined as the process of partitioning an image into mutually exclusive regions based on pixel characteristics. The goal of image segmentation is to assign each pixel to a group or class with similar characteristics. Ideally, classes with similar characteristics correspond to similar objects in an image [1, 26].

If the domain of the image is given by Ω, then the segmentation problem is to determine the sets S_k C Ω whose union is the entire domain Ω. Thus, the sets that make up a segmentation must satisfy: $\Omega = \bigcup_{k=1}^{K} S_k$, where $S_k \cap S_j = \phi$ for $k \neq j$ and each S_k is connected (each cannot be partitioned into two nonempty subsets). Ideally segmentation methods find those sets that correspond to distinct anatomical structures or regions of interest in the image. When the constraint that regions be connected is removed, then determining the sets S_k is called pixel classification, and the sets themselves are called classes. Pixel classification, rather than classical

segmentation, is often a desirable goal in medical images, particularly when disconnected regions belonging to the same tissue class require identification [27]. Determination of the total number of classes K in pixel classification can be a difficult problem. Often, the value of K is assumed to be known based on prior knowledge of the anatomy being considered. For example, in the segmentation of magnetic-resonance (MR) brain images, it is common to assume that K = 3, corresponding to gray-matter, white-matter, and cerebrospinal-fluid tissue classes. The process of assigning a meaningful designation to each region or class, which is called Labeling, is usually done following a successful segmentation. This procedure maps the numerical index k of set S_k to an anatomical designation. When such labels are visually obvious, then it can be determined just through inspection by expert observers (physicians or technicians in the case of medical images, for example [27]). When the labels are not obvious, however, computer automated labeling systems are desirable. A typical situation involving labeling occurs in digital mammography, in which the image is segmented into distinct regions and the regions are subsequently labeled as healthy or tumorous tissue [28].

Image segmentation approaches commonly discussed in the literature include: tresholding, region growing, classifier based, clustering, Markov random fields, artificial neural network, deformable models, and atlas-guided approaches, to mention a few. Detailed discussion on such segmentation approaches is available in ref. [27].

3.3. Spectral analysis of color images

Information content of an image, which are used for various analysis, can be conveyed in spatial or frequency domain. The term spatial domain refers to the image plane itself, and image processing approaches in this domain are based on direct manipulation of pixels in an image. Most image signals in spatial domain are affected due to various artifacts such as noise, poor

image contrast, image acquisition artifacts, signal complexity and redundancy of information. For this reason, it is necessary to analyze an image in a different domain. In this regard, spatial frequency (wave number) transformations have been used in different applications. These include the 2D Fourier transform, the 2D Hartley transform, the 2D cosine transform and the like. Also joint space-wave number transforms have been used in applications requiring local analysis. These include the 2D Gabor transform, the 2D wavelet transform, 2D S transform and the like. The above mentioned transforms were however originally developed to analyze grayscale images where each image pixel is assumed to be real (or in some cases complex) valued. Most color images, however, have at least three components/channels/bands and the application of the above mentioned transforms is then very limited to analyze such images. In this regard, various alternatives have been suggested in the literature for use in analyzing color images with multiple components. Below we will review some of these approaches.

- **Monochromatic analysis**

One way of analyzing color images is to treat the components as separate monochromatic images. In this way, for example the real and complex valued transforms mentioned above could be used to extract the spectral content available in each color channel. The major drawback of such an approach is that it misses out the correlation information embedded among the different channels of the color images. Finding such correlation information after serial analysis is often not obvious. Another drawback is that the monochromatic analysis essentially results in higher computational costs compared to other holistic approaches. It is sometimes possible to transform a given multi component color image into single component grayscale and do the analysis on a new space. There are instances where this method gives satisfactory results for some applications

[28, 29]. Methods that incorporate all color components and the intrinsic inter correlation among the different color components should provide a better approach in handling color images.

- **Complex representation of color images**

Another approach in color image analysis makes use of a representation in the complex space. This is based on converting the original RGB image to HSV color space and considering the hue (H) and saturation (S) components as the phase and the magnitude of the complex form respectively. As explained in [30] an image h(x, y) represented in the RGB color space with three color bands, R(x, y), G(x, y), and B(x, y), can be converted to HSL color space and represented in cylindrical coordinate system with three color bands, H(x, y), S(x, y) and L(x, y). This can be represented in complex form as:

$$h(x,y) = S(x,y)^{iH(x,y)} \tag{3.1}$$

where the saturation, S(x, y), is the magnitude and the hue, H(x, y), is the phase of the complex form. In this way the standard complex Fourier based transforms can be employed to analyze the color values hue and saturation separated from the intensity. However the intensity is not explicitly represented in this form.

- **Representation of color images in the hyper-complex domain**

For effective analysis of color images we need a holistic representation technique of all the color channels. In this regard, holistic color image analysis techniques in the hyper-complex space using quaternions and more recently using the three space numbers known by the name trinions have been suggested in the literature [31, 32]. A quaternion has one real and three imaginary components [31]. A quaternion number q can be written as:

$$q = a + ib + jc + kd \tag{3.2}$$

where a, b, c and d are real numbers and i, j and k are orthonormal operators satisfying the following multiplication rules:

$$ij = k, \qquad jk = i, \qquad ki = j \tag{3.3}$$

$$ji = -k, \qquad kj = -i, \qquad ik = -j$$

Quaternions have been used to efficiently represent color images as one object/entity and the respective Fourier transforms defined in the quaternion spaces stimulated several useful applications in various areas of image analysis [33].

Most color images have three components and one drawback of use of quaternions in representing and analyzing such color images is the extra fourth dimension that quaternions posses which creates redundancy. That means quaternion representation of color images is not unique. A recent work in the field of color image processing aimed to circumvent the issue of this redundancy that we incur using the quaternion formulation. New numbers in the three space known by the name trinions have been suggested recently for a unique representation and efficient analysis of color images with three components [32].

The three components of a given color image can be mapped to the three components of a trinion there by avoiding the redundancy issue we incurred using the quaternion representation. The introduction of the trinions has stimulated useful applications in analyzing multi-component medical images (see [33] for example). It is the intent of this thesis to discuss more in detail about trinions and their applications in analyzing retinal images generated based on fundus cameras for use in studying a complication of diabetics known by the name diabetic retinopathy.

3.4. Fundus retinal image analysis

As it is mentioned in chapter one, in clinical ophthalmology use of computer aided fundus image analysis techniques for diagnosis of DRs enable effective screening and monitoring of abnormalities in the retina. But there are lots of challenges in designing schemes for use in automated retinal image analysis. This is due to the fact that fundus images are usually affected by various artifacts. Some of the common factors, which usually make retinal image analysis a hard task, are presence of noise, poor image contrast, presence of anatomical structures with highly correlated pixels with that of lesion, illumination variability, color variation of similar subjects due to difference in background, size and shape variation of lesions, and eye movement during image acquisition. Various methods have been suggested in the literature for automatic segmentation of pathological and anatomical structures of color retinal images. Due to retinal pigmentation and the acquisition process, the retinal images vary largely in luminosity and contrast, making it harder to distinguish retinal features and lesions in some areas thus hindering the automatic segmentation of abnormalities. Most automatic systems approach the detection of eye diseases directly using shape, color, texture, and domain knowledge of abnormality findings. Selection of those top most representative features enables to mimic the way how experts identify the presence of abnormalities, such as DR and glaucoma, in the retina. Literatures in [34-38] differentiate EX pixels from non-EX pixels by extracting some of these relevant and significant features. Other techniques attempt to find abnormalities indirectly by detecting changes between two fundus images taken from the same eye in different time moment. The direct approaches contribute to screening of the disease, where as indirect approaches contribute to both screening and monitoring of the existed abnormalities [20].

Generally most image analysis techniques for finding abnormalities in fundus images have three major stages. Those stages are preprocessing (or image enhancement), candidate abnormality detection and classification to correct finding category. Most of the automatic methods also detect normal fundus parts, such as the OD, blood vessels, and the macula. These methods either use the vital domain information provided by the normal fundus parts or remove them due to their similar color and shape appearance with abnormal fundus findings. For instance an automated blood vessel segmentation method can be a suitable tool for being integrated into a complete pre-screening system for early DR detection. Localization of OD either in the presence or absence of HE is another method used for the purpose of DR detection [20, 34, 35]. Others proposed blood vessel segmentation and fovea localization for the same purpose [38-42]. Other schemes focus on detection and grading of EXs for diagnosis of DR [43]. In fact most analysis techniques are applied to specific objectives. It is not possible to detect all types of abnormality in fundus using a single algorithm.

The sections below review some literatures done in the area of fundus image processing and the various related works done so far in terms of their algorithm, specific methodological stages, and type of disease identification scheme.

3.4.1. Overview of preprocessing methods used in fundus image analysis

Patient movement, poor focus, bad positioning, reflections, inadequate illumination can cause a significant proportion of images to be of such poor quality as to interfere with analysis [44, 45]. In approximately 10% of the retinal images, artifacts are significant enough to impede human grading [45]. Preprocessing of such images can ensure adequate level of success in the automated abnormality detection. In the retinal images there can be variations caused by the factors including differences in illumination, acquisition angle and retinal pigmentation. First

step in the preprocessing is to attenuate such image variations by normalizing/matching the color of the original retinal images against a reference image (an image that is taken under good imaging conditions) by using some histogram specification techniques. Retinal images typically have a higher contrast in the centre of the image with reduced contrast moving outward from the centre. Different preprocessing methods have been suggested in the literature to overcome these problems.

Image normalization techniques are used to reduce the effect of unwanted image variations between subjects by using histogram matching against a reference image [42, 44]. However those histogram matching techniques may also lead a loss of important information in the original image. For instance small number of HEs that have relatively less amount of brightness may be considered as an artifact and suppressed in the histogram matching process. To correct for non uniform background illumination, mean and median filters are also used in the green channel of the original image by some researchers [20, 34]. In other literatures the image is divided into non overlapping rectangular regions and the mean and standard deviation of those windows are used to estimate the background [44, 45]. The techniques were applied on the intensity channel. The same approach has also been applied on the H channel in the HSV color space [46]. Other studies proposed global and local contrast enhancement techniques to improve the contrast of the original image. This procedure enhances visualization and segmentation of abnormalities in fundus images. One method suggested, for example, uses contrast limited adaptive histogram equalization (CLAHE) [43]. Other preprocessing techniques apply noise estimation (removal) techniques such as back ground noise suppression and mask estimation [45].

Selection of best color spaces that have maximum interclass separablity for abnormality types is also a major preprocessing task. In [35] the green channel from the RGB color space was chosen for further analysis. Similarly the intensity component from the HSV color space was selected in [37]. In [41] the LUV color space was chosen. A multi channel processing based on the green (from RGB), lightness (from LUV), and magenta (from CMYK) color combinations has also been used for efficient analysis [34].

Generally, most fundus images are characterized by being low contrast and infested with image artifacts which are signified by the grouping of large peaks in a small area on the histogram plot [44]. See Fig. 3.3 for example. This to a great extent interferes with the image analysis process. The aim of preprocessing is then to attenuate the effect of such unwanted artifacts, keeping the vital information. However, unless we have optimum preprocessing schemes that best suit for optimum feature extraction and classification result, it may lead to additional error and degradation to the total algorithm performance. There is always a problem to balance the tradeoff between the need for preprocessing step and its drawbacks.

3.4.2. Candidate abnormality detection and classification techniques

As said before, the three major steps often used for the purpose of feature based object segmentation are feature extraction, followed by candidate abnormality estimation, and finally classification. Various researches have been done in automated segmentation of pathological and anatomical structures of retinal images, such as EXs, retinal blood vessels, fovea, macula and OD. Some of these include filter based, vessel tracking, classifier based and morphological methods. The techniques utilize the prior knowledge such as contrast that exists between the blood vessels and surrounding background, color and shape information.

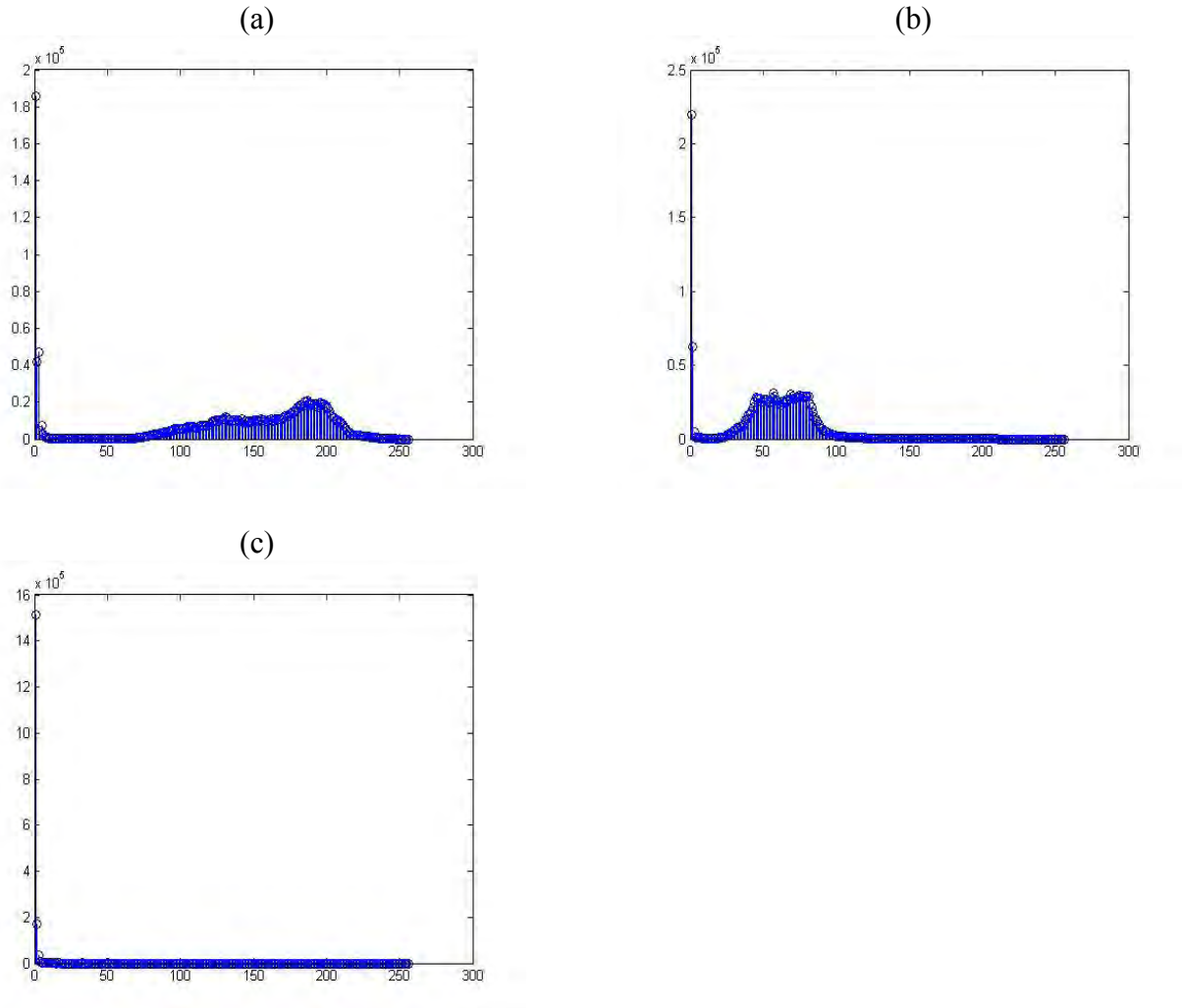

Figure 3.3: Histogram plot of a sample fundus image for its red channel (a), green channel (b), and blue channel (c).

Exudate detection and segmentation

As EXs are among common early clinical signs of DR, their detection would be an important asset to the mass screening tasks and could serve as a first step towards a complete monitoring and grading of the disease. Some researchers attempted to detect EXs by using tresholding techniques [47-49]. However, the wide variability among retinal images makes those methods dependent on user intervention to select the appropriate threshold for each case. The authors in [47] combined global and local tresholding to segment EXs. But their method requires a priori

knowledge about the location of EXs. For the same purpose the authors in [48] proposed a local dynamic tresholding algorithm. In [49] a multi-level tresholding method is employed to EXs segmentation. However, the method was applied on very small samples and generalizations were hard to be reached.

One primary problem with the tresholding approaches is that it is difficult to automatically find an adaptive threshold that accounts for local image variations. In that regard, there are other approaches suggested in the literature. Some researchers used a recursive region growing segmentation algorithm (RRGS) to achieve automatic detection of EXs in retinal images [50]. Their method used tresholding based on the homogeneity of the EXs illumination. Other researchers combined the region growing technique with edge detection [51]. Their method is implemented on LUV color space. In their algorithm, seeds in a sub image are selected first. The pixels adjacent to a seed are tested, and the region is allowed to grow from the seed until reaching an edge or large gradient detected by canny edge detector.

Generally, the region growing techniques are time consuming and probably result in under-segmentation and over-segmentation situations. In [36] authors created a model of the retina to automatically identify the presence of lesions in the macular region. Edge and brightness information were combined in [37] to identify EXs and the severity of DR. However, these studies did not explicitly address the differentiation among lesion types. Other methods include Bayesian classifiers [52], KNN classifier followed by LDA [53], NN based classifiers [54-56], Fuzzy C-means clustering [55], and SVM classifiers [55, 56].

Authors in [57] proposed a novel approach of segmenting EXs for screening and follow–ups by building an ethnicity based statistical atlas. The chromatic distribution in such an atlas gives a

good measure of probability of the pixels belonging to the healthy retinal pigments or to the abnormalities (like lesions, imaging artifacts etc.) in the retinal fundus image. Post–processing schemes were also introduced for the enhancement of the edges of such EXs for final segmentation and to separate lesion from false positives. But the major limitation was that the statistical atlas reference cannot represent all the variables within the world population. In [37] the authors proposed an automated retinal image analysis technique to detect and quantify lesions associated with DR. The work focused on automatic detection of one lesion type associated with DR (the HEs) based on an algorithm that uses a statistical classification approach combined with an edge detection scheme for edge localization. The assumption here was that HEs appear in the fundus photographs as small yellow white patches with sharp margins and different shapes. Nevertheless, the result presented by the authors indicated poor sensitivity by their proposed algorithm.

Other researchers in [58] came up with automatic EX detection using fuzzy C-means and morphological methods. The process has two main segmentation steps which are coarse segmentation using fuzzy C-means clustering and fine segmentation using morphological reconstruction. Four features, namely intensity, standard deviation of intensity, hue, and adapted edge were selected for coarse segmentation. Another novel automated approach for detecting HEs is proposed in [20]. The algorithm is based on Fisher's LDA and makes use of color information to perform the classification of EXs. However the proposed algorithm makes use of the isolated EXs color to characterize yellowish regions. A limitation of this approach is that it cannot represent the color of all the EXs found in color retinal images. Additionally, despite the enhanced appearance of the HEs brought about by the preprocessing techniques, their diversity in brightness and size makes it difficult for an automatic algorithm to detect all of them. HEs

usually appear in groups and therefore missing some of the very faint EXs is often believed not to be critical. However, when there are only few very faint HEs in the retina, the algorithm will have limited performance.

Researchers in [46] presented retinal image analysis based on mixture models to detect and segment HEs by dynamically tresholding the images in order to separate the EXs from the background. A post processing technique, based on edge detection, is applied to distinguish HEs from CW spots and other artifacts. Another automatic localization and segmentation of HEs using mathematical morphology operations was proposed in [35]. In this work, the retinal images were first preprocessed and the OD and the blood vessels were identified and then they were eliminated from the image. Finally, the HEs were segmented by a mixture of different morphological operations including the top-hat, bottom-hat, and reconstruction operations.

Automatic segmentation of HEs has also been done previously using radial basis function network in [59] and SVM in [60]. The SVM algorithm was based on the Discrete Cosine Transform (DCT) analysis and SVM was used for the purpose of classifying the retinal EXs. It attempts to mimic the ophthalmologist expertise by extracting relevant and significant features. Features are empirically selected and used as input for SVM clustering. The major limitation of this learning algorithm was that the result deteriorates for a bulk of unseen data set.

Blood vessel segmentation

Since vessels serve as one of the main retinal landmark features, blood vessel segmentation is also the basic foundation while developing retinal screening systems. Authors in [39] came up with an automatic blood vessel segmentation technique in retinal images. The method utilized a tracking algorithm based on level sets and Fast Marching methods. However the tracking algorithm fails in special cases on abnormal images: they are often sidetracked by light objects

and sometimes experience difficulty locating starting points so that its levels of success is frequently inadequate for wide scale implementation. Authors in [40] also proposed an automated method for identification of blood vessels in color images of the retina. For every image pixel, a feature vector is computed that utilizes properties of scale and orientation selective Gabor filters. The extracted features are then classified using generative Gaussian mixture model and discriminative SVM classifiers. Algorithm for automatic segmentation of blood vessels has also been done by using vessel enhancement techniques and Fast Marching method [41]. The algorithm includes the following major steps: Morlet wavelet transform, curvature estimation, matched filtering, and Fast Marching. The wavelet transform and the curvature-based approach were first applied to detect the skeleton of vessels, which serve as the initial seeds in the Fast Marching algorithm. The matched filter is then used to enhance the vessels in order to extract the features used by the Fast Marching's velocity function. Finally, the Fast Marching algorithm is applied to obtain final segmentation of retinal blood vessels.

A hybrid method for efficient segmentation of multiple oriented blood vessels was done in [42]. Initially, the appearance of the blood vessels were enhanced and back-ground noise is suppressed with the set of real component of a complex Gabor filter. Then the vessel pixels were detected in the vessel enhanced image using entropic tresholding based on GLCM as it takes into account the spatial distribution of gray levels and preserving the spatial structures. This method is comprised of two steps that is the retinal vessel enhancement followed by entropic tresholding. A set of Gabor filters tuned to particular frequency and orientation are used to enhance the blood vessels suppressing the background. In another work, automatic segmentation of retinal vessels by using Zhang's method has been proposed [38]. In this method an active contour was used to

extract vessel networks from color retinal images. This automatic analysis of retinal vessels facilitates calculation of arterial index which is required to diagnose certain retinopathies.

Severity grading of eye diseases due to DR

An automated algorithm to detect and grade the severity of HEs is done in [37]. The detection process was based on top-down image segmentation and local tresholding by a combination of edge detection and region growing. Using features of the fovea and their geometric relations with other retinal structures, a method for the fovea localization was proposed [46]. Grading of HEs was performed using a polar coordinate system centered at the fovea [37, 46].

An efficient detection of the OD in color retinal images is also a significant task in an automated retinal image analysis system. Most of the algorithms developed for OD detection/localization are especially applicable to healthy retinal images. It is a challenging task to automatically segment OD in abnormal retinal images. The position of OD can be used as a reference length for measuring distances in retinal images, especially for the location of the macula. In case of blood vessel tracking algorithms, the location of OD have been used as the starting point for vessel tracking [39].

Most of the above methods proposed for different uses in retinal image processing share one common property: one way or the other they all require color component separation. As mentioned previously, such an approach misses out the intrinsic correlation information that is embedded among the color bands and this information is proved to be vital in different applications of color image analysis. Unlike most of the former works, authors in [34] proposed an approach that combined three representative channels to form novel features. Based on the multichannel features, they employ boosted soft segmentation (BSS) algorithm to obtain a

confidence map, and then apply a background subtraction method to get the coarse segmentation result. The selected three channels were green from RGB color space, luminosity from LUV color space and magenta from CMYK color space. Then CLAHE is applied to the selected three channels for contrast enhancement. The channels were selected based on observation for effective extraction of HEs. The limitation of this approach is the challenge of selecting the effective channels that best suit for the BSS algorithm. Additionally it only works for detection of HEs.

It is the intent of this thesis to propose a method to overcome the shortcomings of most of the methods proposed so far. The new approach is primarily holistic in that it employs vectorial representation of color pixels based on a solid mathematical concept. It applies extraction of meaningful higher order features based on integral transforms defined in higher dimensional spaces. Robust feature selection guarantees superior object detection capabilities. In the next chapters the new scheme will be discussed in detail and its efficacy in effective detection/segmentation and classifications of useful objects in fundus generated retinal images will be demonstrated subsequently.

References

1. R. C. Gonzalez, R. E. Woods, Digital Image Processing, Pearson Education, 3rd Edition, 2002.
2. K. A. Thomas, Image processing as applied to medical diagnostics, MSc dissertation, University of Oregon, 2010.
3. P. J. Baldevbhai and R. S. Anand, Color Image Segmentation for Medical Images using L*a*b* Color Space, J. Eletronic. Comm. Eng., 1(2), pp. 24-45, 2012.
4. H. D. Cheng, X. H. Jiang, Y. Sun, and J. L. Wang, Color image segmentation: advances and prospects, Pattern Recognition, 34(12), pp. 2259-2281, 2001.
5. C. H. Wei, C. T Li, and R. Wilson, Content Based Approach to Medical Image Database Retrieval, pp. 259-291, 2006.
6. S. L. Michael, Principles of visual information retrieval, Springer, pp. 11-49, 2001.
7. C. H. Li and T. Yuen, Regularized color clustering in medical image database, IEEE Transaction on Medical Imaging, 19(11), pp. 1150-1155, 2000.
8. A. Ouyang and Y. P. Tan, A novel multi-scale spatial-color descriptor for content-based image retrieval, Proc. Int. Conf. Contr. Autom. Rob. Vis., 3, pp. 1204-1209, 2009.
9. H. Yu, M. Li, H-J. Zhang, and J. Feng, Color texture moments for content-based image retrieval, Proc. Int. Conf. Image Proc.. Vol. 3 , pp. 929-932, 2002.
10. T. Gevers and H. Stokman, Classifying color edges in video into shadow-geometry, highlight, or material transitions, IEEE Trans. Multimedia, 5(2), pp. 237-243, 2003.
11. H. Guan and S. Wada, Flexible color texture retrieval method using multi resolution mosaic for image classification, Proc. Int. Conf. Signal Proc., Vol. 1 , pp. 612-615, 2002.
12. H. A. Moghaddam, T. T. Khajoie, and A. H. Rouhi, A new algorithm for image indexing and retrieval using wavelet correlogram, Proc. Int. Conf. Image Proc., Vol. 3, pp. 497-500, 2003.
13. M. Nishibori, Problems and solutions in medical color imaging, Proc. Int. Symp. Multi-Spectral Imaging and High Accurate Color Reproduction, pp. 9-17, 2000.
14. J. Sahar, S. Zahra, and C. A. Mehdi, A Robust Brain MRI Classification with GLCM Features. Int. J. of Comp. Appl., 37(12), pp. 1-5, 2012.
15. V. P. Gladis, P. Rathi and D. S. Palani, A novel approach for feature extraction and selection on MRI images for brain tumor classification, J. Know. Data Eng., 13(2), pp. 714-720, 2004.

16. A. K. Wing, Partial Differential Equation Based Methods in Medical Image Processing, PhD dissertation, Coventry University, Philippines, August 2007.
17. O. Egecioglu, H. Ferhatosmanoglu, and U. Ogras, Dimensionality reduction and similarity computation by inner-product approximations, IEEE Transact. Know. Data Eng., 16(6), pp. 714-726, 2004.
18. M. Partridge and R. Calvo, A fast dimensionality reduction and simple PCA, Intel. Data Anal., 2(1-4), pp. 203-214, 1998.
19. U. Sinha and H. Kangarloo, Principal component analysis for content based image retrieval, RadioGraphics, 22, pp. 1271-1289, 2002.
20. C. I. Sanchez, R. Hornero, M. I. Lopez, C. M. Aboy, C. Poza , and D. Abasolo, A novel automatic image processing algorithm for detection of hard exudates based on retinal image analysis, Medical Engineering & Physics, Vol. 30 , pp. 350 -357, 2008.
21. G. D. Tourassi, Journey toward computer-aided diagnosis: Role of image texture analysis, Radiology, pp. 317-320, 1999.
22. D. Assefa, H. Keller, C. Manard, N. Laperriere, R. J. Ferrari, and I. Yeung, Robust texture features for response monitoring of glioblastoma multiforme on T1-weighted and T2-FLAIR MR images: A preliminary investigation in terms of identification and segmentation, Med. Phys., 37(4), pp. 1722- 1736, 2010.
23. M. Singh, M. Markou, and S. Singh, Color image texture analysis: Dependence on color space, Pro. IEEE Int. Conf. Pattern Recogn., Quebec City (QC, Canada), Vol. 1, pp. 672-676, 2002.
24. R. S. Choras, Image Feature Extraction Techniques and Their Applications for CBIR and Biometrics Systems, 1(1), 2007.
25. A. K. Jain, R. P. W. Duin, and J. Mao, Statistical Pattern Recognition: A Review, IEEE Trans. Pattern Anal. Mach. Intel., 22(1), 2000.
26. C. Solomon and T. Breckon, Fundamentals of Digital Image Processing, 2nd edition, Wiley-Blackwell, 2011.
27. D. Pham, C. Xu, and J. L. Prince, Current methods in medical image segmentation, Annu. Rev. Biomed. Eng., Vol. 2, pp. 315-337, 2000.
28. M. Vasantha, V. S. Bharathiah, R. Dhamodhara, Medical Image Feature Extraction, Selection and Classification, Int. Jour. Eng. Sci. Tech., 2(6), pp. 2071-2076, 2010.

29. W. E. Polakowski, D. A. Cournoyer, S. K. Rogers, M. P. Dedsimio, D. W. Ruck, Computer-aided breast cancer detection and diagnosis of masses using difference of Gaussians and derivative-based feature saliency, IEEE Trans. Med. Imaging, Vol. 16, pp. 811–819, 1997.
30. D. Assefa, The 1D and 2D Localized Hartley Transforms their Parallel Implementation and Applications; Color Image Analysis Using Quaternions and Trinions, Phd. dissertation, University of Western Ontario, London, Ontario, 2007.
31. D. Assefa, L. Mansinha, K. F. Tiampo, H. Rasmussen, and K. Abdella, Local quaternion Fourier transform and color image texture analysis, Signal Processing, 90(11), pp. 1825-1835, 2010.
32. D. Assefa, L. Mansinha, K. F. Tiampo, H. Rasmussen, and K. Abdella, The trinion Fourier transform of color images, Signal Processing, 91(8), pp. 1887-1900, 2011.
33. D. Assefa, H. Keller, and D. A. Jaffray, Multi-parametric MR image processing using higher dimensional vector algebra, ISPHT, Washington, DC, USA, pp. 24-31, 2011.
34. H.-C. Lu and G.-L. Fang, An effective framework for automatic segmentation of hard exudates in fundus image, J. Circuit Syst. Comp, 22(1), 2013.
35. M. Ghafourian, F. Eadgahi, and H. Pourreza, Localization of HE in retinal fundus image by mathematical morphology operation, J. Theoretical phys. Cryptography, 1(11), 2012.
36. G. B. Kande, P. V. Subbaiah, and T. S. Savithi, Feature extraction in digital fundus image, J. Medical and Biological Engineering, 29(3), pp. 122-130, 2009.
37. C. I. Sanchez, R. Hornero, M. J. Lopez and J. Poza, Retinal image analysis to detect and quantify lesions associated with diabetic retinopathy, Conf. Proc. IEEE Eng. Med. Bio. Soc., pp. 1624-1627, 2004.
38. E. Saghapour, and S. Zandian, Automatic segmentation of retina vessels by using Zhang method, World Academy of Science, Engineering and Technology, Vol. 72, pp. 12-23, 2012.
39. P. Echevarria, T. Millerr and J. Omeara, Blood vessel segmentation in retinal images, 2004.
40. A. Osareh and B. Shadgar, Automatic blood vessel segmentation in color images of retina, I. J. Sci. Tech. Trans. Eng., 33(B2), pp. 191-206, 2009.
41. C. Liu, H. Lu and J. Zhang, Using fast marching in automatic segmentation of retinal blood vessels, IFMBE Proceedings, Vol. 19, pp. 233-236, 2010.
42. P. C. Siddalingaswamy, K. G. Prabhu, Automatic detection of multiple oriented blood vessels in retinal images, J. Biomedical Science and Engineering, 3(1), pp. 101-107, 2010.

43. H. Jaafar, K. N. Asoke, and W. Al-Nnuaimy, Automated detection and grading of hard exudates from retinal fundus images, European Signal Proc. Conf., pp. 66-70, 2011.
44. I. Jamal, M. A. Usman, and A. Tariq, Retinal image preprocessing: background and noise segmentation, TELKOMNIKA, 10(3), pp. 537-544, 2012.
45. A. Tariq and M. A. Usman, An Automated System for Colored Retinal Image Background and Noise Segmentation, ISIEA, Penang, Malaysia, pp. 423-427, 2010.
46. C. I. Snchez, M. Garca, A. Mayo, M. I. Lopez, and R. Hornero, Retinal image analysis based on mixture models to detect hard exudates, Med Image Anal., 13(4), pp. 650-658, 2009.
47. R. Phillips, J. Forrester and P. Sharp, Automated detection and quantication of retinal exudates, Graefes Arch. Clin. Exp. Ophthalmol., 231(2), pp. 90-94, 1993.
48. D. Kavitha and S. S. Devi, Automatic detection of optic disk and exudates in retinal images, Proc. Int. Conf. Intelligent Sensing and Information Processing, Chennai, India, pp. 501-506, 2005.
49. Z. Liu, O. Chutatape and S. M. Krishnan, Automatic image analysis of fundus photographs, IEEE Eng. Medicine Biol. Soc., Chicago, pp. 524-525, 1997.
50. C. Sinthanayothin, J. F. Boyce, T. H. Williamson, H. L. Cook, E. Mensah, S. Lal and D. Usher, Automated detection of diabetic retinopathy on digital fundus images, Diabetic Medicine, Vol. 19, pp.105-112, 2002.
51. H. Li and O. Chutatape, Automated feature extraction in color retinal images by a model based approach, IEEE Trans. Biomed. Eng. Vol. 51, pp.246-254, 2004.
52. B. M. Ege, O. K. Hejlesen, O. V. Larsen, K. Moller, B. Jennings, D. Kerr, and D. A. Cavan, Screening for diabetic retinopathy using computer based image analysis and statistical classification, Comput. Methods Programs Biomed., Vol. 63, pp. 165–175, 2000.
53. M. Niemeijer, B. V. Ginneken, S. R. Russell, M.S. A. Suttorp-Schulten, and M. Abramoff, Automated detection and differentiation of drusen, exudates, and cotton-wool spots in digital color fundus photographs for diabetic retinopathy diagnosis, Invest. Ophthalmol. Vis. Sci., Vol. 48 , pp. 2260-2267, 2007.
54. G. G. Gardner, D. Keating, T. H. Williamson, A. T. Elliot, Automatic detection of diabetic retinopathy using an artificial neural network: a screening tool, British J. Ophthalmol., Vol. 80, pp. 1-5, 1996.

55. X. Zhang, and O. Chutatape, Top-down and bottom-up strategies in lesion detection of background diabetic retinopathy, Proc. IEEE Computer Soc. Conf. Computer Vis. Pattern Recogn., San Diego, CA, USA, pp. 181-186, 2005.
56. A. Osareh, Automated identification of diabetic retinal exudates and the optic disc, PhD dissertation, Bristol, 2004.
57. S. Ali, K. M. Adal, D. Sidib, T. P. Karnowski, E. Chaum, and F. Meriaudeau, Exudates segmentation on retinal atlas space, 2002.
58. A. Sopharak, B. Uyyanonvara, Automatic exudates detection from diabetic retinopathy retinal image using fuzzy c-means and morphological methods, Proc. Int. Conf. Computer Sci. Tech., Phuket, Thailand, pp. 359-364, 2007.
59. R. Vijayamadheswaran, M. Arthanari, and M. Sivakumar, Detection of diabetic retinopathy using radial basis function, Int. J. Innovative Tech. Creative Eng., 1(1), pp. 40-47, 2011.
60. K. Wisaeng, N. Hiransakolwong, and E. Pothiruk, Automatic detection of retinal exudates using a support vector machine, Applied Medical Informatics, 32(1), pp. 33-42, 2013.

Chapter four

4. A novel, holistic color retinal image analysis

4.1. Method of retinal image acquisition

A fundus camera or retinal camera is a specialized low power microscope with an attached camera designed to photograph the interior surface of the eye, including the retina, OD, macula, and posterior pole (the fundus). The retina can be photographed directly as the pupil is used as both an entrance and exit for the fundus camera's illuminating and imaging light rays. The patient sits at the fundus camera with their chin in a chin rest and their forehead against the bar. An ophthalmic photographer focuses and aligns the fundus camera. A flash fires as the photographer presses the shutter release, creating a color fundus photograph. Ophthalmologists use these retinal photographs for diagnosis, treatment, and subsequent follow ups of eye diseases.

Compared to other retinal imaging techniques, for instance OCT and hyper spectral imaging techniques, fundus photography generally needs a considerably cheaper instrument. Fig. 4.1 shows a typical fundus camera design. It has the advantage of availing the image to be examined by a specialist at another location and/or time, as well as providing color photo documentation for future reference. It provides an upright, magnified view of the fundus with 30 to 50 degrees field-of-view of retinal area. A typical camera views 30 to 50 degrees of retinal area, with a magnification of 2.5x, and allows some modification of this relationship through zoom or auxiliary lenses from 15 degrees which provides 5x magnification to 140 degrees with a wide angle lens which minifies the image by half [1, 2].

Figure 4.1: Fundus camera. Courtesy of Sain et al.

- **Optical principles of fundus camera**

The optical principles of fundus camera are similar to the principles of monocular indirect ophthalmoscopy in that the observation and illumination systems follow dissimilar paths [1]. Light generated from either viewing lamp or the electronic flash is projected through a set of filters and onto a round mirror. This mirror reflects the light up into a series of lenses which focus the light. A mask on the uppermost lens shapes the light into a doughnut. The doughnut shaped light is reflected onto a round mirror with a central aperture, exits the camera through the objective lens, and proceeds into the eye through the cornea. Assuming that both the illumination system and the image are correctly aligned and focused (as shown in Fig. 4.2), the resulting retinal image exits the cornea through the central, un-illuminated portion of the doughnut. The light continues through the central aperture of the previously described mirror, through the astigmatic correction device and the diopter compensation lenses, and then back to the single lens reflex camera system. Fig. 4.3 shows a general schematic diagram of the light rays' path in fundus camera [1].

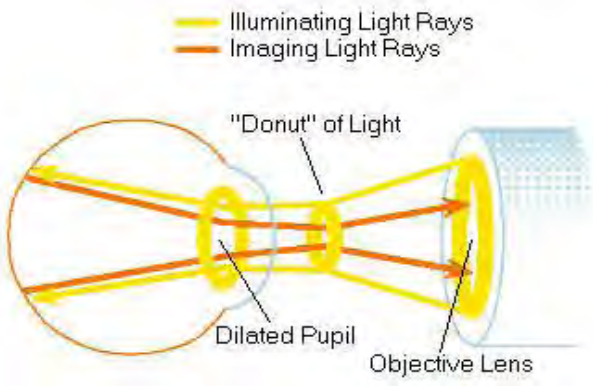

Figure 4.2: Ideal paths of illumination and observing/imaging light rays. Courtesy of Sain et al.

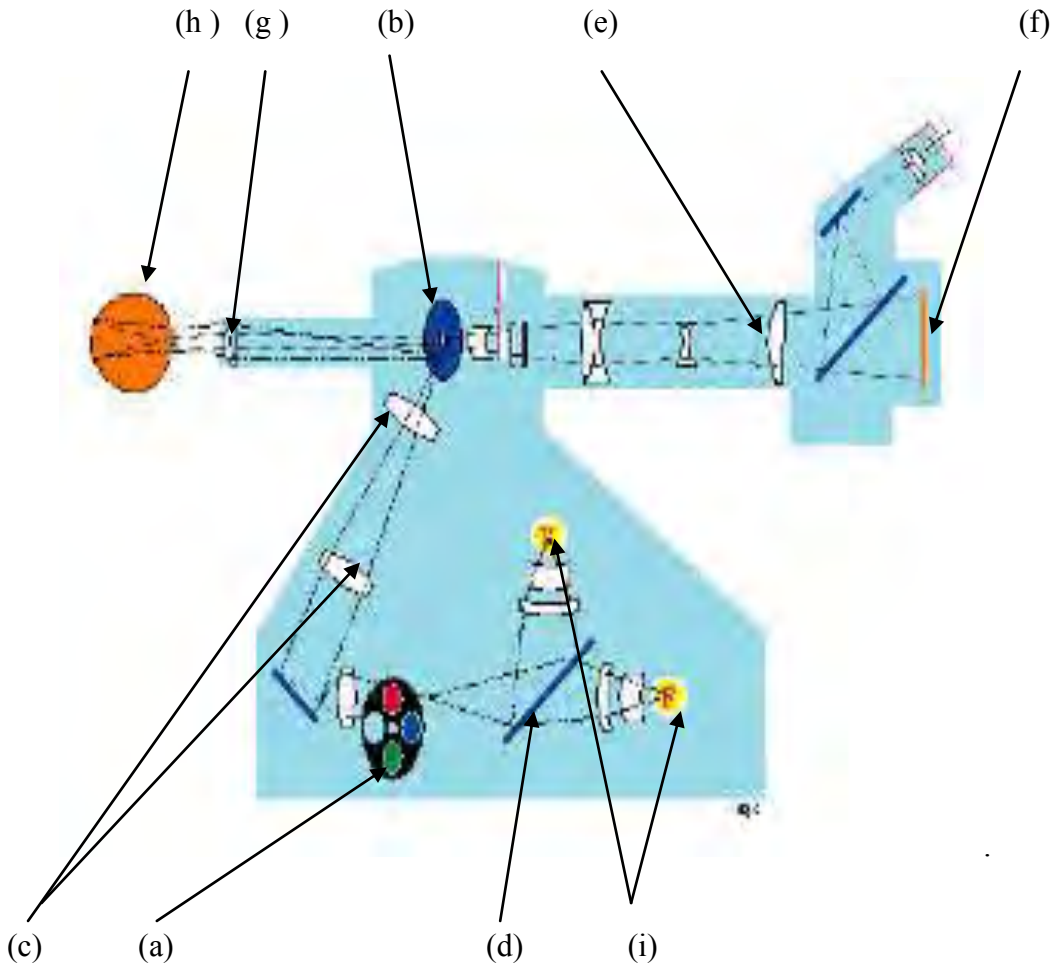

Figure 4.3: Schematic diagram of fundus camera optics, round mirror (a), Donut of light (b), lenses to focus light (c), mirror (d), diopter compensation lens (e), camera detector or CCD (f), objective lens (g), eye (h), light source (i). Courtesy of Sain et al.

4.2. Data sets

The following publicly available standard data sets have been used in the current work:

- DIARETDB0: 130 color fundus images, 10 are normal and 120 contain mild non-proliferative DR with the annotation from the experts.
- DIARETDB1: 89 color fundus images of which 5 are normal and 84 contain non-proliferative DR with the annotation from the experts.
- High-Resolution Fundus (HRF) image database: contains 15 normal, 15 patients with DR, and 15 glaucomatous patients; binary gold standard vessel segmented images are available.
- STARE (STructured Analysis of the REtinal image) database: contains 81 images; binary gold standard vessel segmented images are available.
- DRIVE (Digital Retinal Image for Vessel Extraction) dataset: contains 40 images; binary gold standard vessel segmented images are available.

The databases are composed of high quality images accompanied by useful medical findings. The expert's delineations are used as gold standards for performance evaluation as well as to carry out comparisons among different segmentation schemes.

Nature of image data sets:

DIARETDB0 and DIARETDB1 images were taken in the Kuopio University Hospital, Kuopio, Finland. The images include the ground truths about the DR findings corresponding to the delineations by the medical experts. The images were selected by the medical experts, but their distribution does not correspond to any typical population, i.e., the data is biased and no a priori information can be devised from it. The DR abnormalities in the database are relatively small, but they appear near the macula which is considered to threaten the eyesight. Images were

captured with the same 50 degree field-of-view digital fundus camera with varying imaging settings (flash intensity, shutter speed, aperture, and gain) controlled by the system. The images contain a varying amount of imaging noise, but the optical aberrations (dispersion, transverse and lateral chromatic, spherical, field curvature, coma, astigmatism, distortion) and photometric accuracy (color or intensity) are the same [3,4]. Therefore, the system induced photometric variance over the visual appearance of the different retinopathy findings can be considered as small. Both image data sets correspond to a good practical situation, where the images are comparable, and can be used to evaluate the general performance of diagnostic methods. The patient information from both databases was removed by converting the images into raw data. The raw data images were converted to lossless portable network (.png) images for the purpose of transmission and storage. The images are typically 24 bit RGB with dimension of 1500x1115 pixels. A special software tool was provided for the experts to inspect the fundus images and annotate their findings. The experts were asked to mark the areas related to the MA, H, HE and SE. They were further instructed to report their confidence and especially annotate the single most representative point for each finding. The ground truth confidence levels, < 50%, > 50%, 100% represented the certainty of the decision that a marked finding is correct. They were taught to use an image annotation tool, but they were not instructed how to make the annotations to prevent a biased scheme. The medical experts learnt their own best practices. The image annotation tool includes the following graphical directives: centroid, polygon region, circle region, ellipse region, and representative point. The expert knowledge gathered with the ground truth tool is stored to a text file. Each line in the text file corresponds to a visual finding marked with the ground truth tool. Each marking in image is defined by the centroid and one other graphical directive [3, 4].

Since the uninstructed collection process caused significant differences between the medical experts, it was not possible to use the expert information as such as the ground truth. However, using the original data the expert knowledge was fused for a better spatial accuracy and suppression of outliers. The fusion was performed on a pixel basis using the reported confidence levels. Several different approaches for fusing the markings are possible, e.g., voting, minimum, maximum and the sum (average) of confidences. The first three provide binary classifications, but the normalized average provides values in the range [0, 1]. Not to discard any information, the approach using the average was selected since it provides a linear confidence scale [3, 4]. In DIARETDB0 and DIARETDB1 the confidence level was fixed to 0.75. The markings reveal how the medical experts analyze and interpret the retinopathy from the digital fundus images. As a demonstration, Fig. 4.4 shows a ground truth for HE based on the above methods.

The STARE data set contains around 81 raw images in portable pixel map (.ppm) format. The images are 24 bit RGB with dimension of 605x500. The dataset contains images which are labeled by hand, to produce ground truth vessel segmentation [5]. All images in DRIVE database are digitized using a Cannon CR5 non-mydriatic 3CCD camera system with a 45 degree field-of-view. Each image is 24-bits per pixel with dimension 565 x 584. These images were labeled by hand, to produce ground truth vessel segmentation. The HRF image data sets are in .jpg format with dimension of 3504x2236.

In addition 80 local images of 20 patients from black lion hospital diabetic center, Addis Ababa, Ethiopia, which include normal images and abnormal images due to non-proliferative DR (HE and H), proliferative DR, glaucoma and Cataract, were collected. However, the local data sets were all in bitmap (.bmp) formats which makes it difficult to perform further processing, and no ground truth were available.


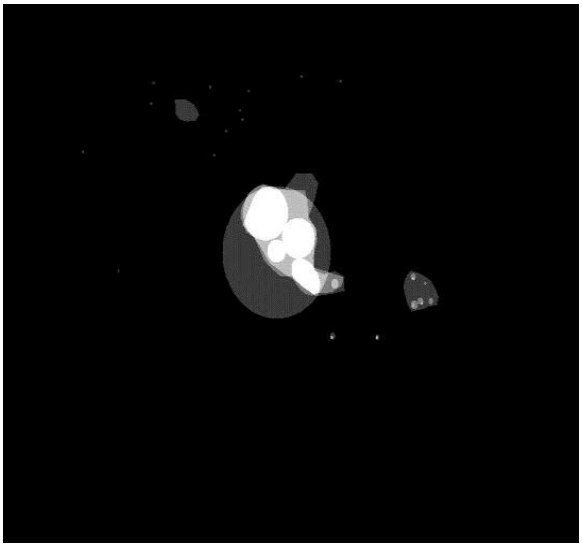

Figure 4.4: Example of an abnormal fundus image from DIARETDB1 database (left), and the available ground truth showing the delineated hard exudates (right).

4.3. Proposed method of image analysis

The proposed methodology as illustrated in Fig. 4.5 focuses on the following two issues:

- Effective enhancement of EXs, Hemorrhages, the OD, and blood vessels based on feature maps generated by means of extracting robust texture descriptors.
- Accurate segmentation of EXs based on a chosen classification scheme.

The proposed scheme uses a holistic representation of the color images in the three (trinion) space and applies trinion based Fourier transforms to extract useful imaging features for the purpose of classification and segmentation of retinal images. A suitable color space transformation and a way of extracting robust higher order features are included in the method. The subsequent sections below discuss the proposed method in detail.

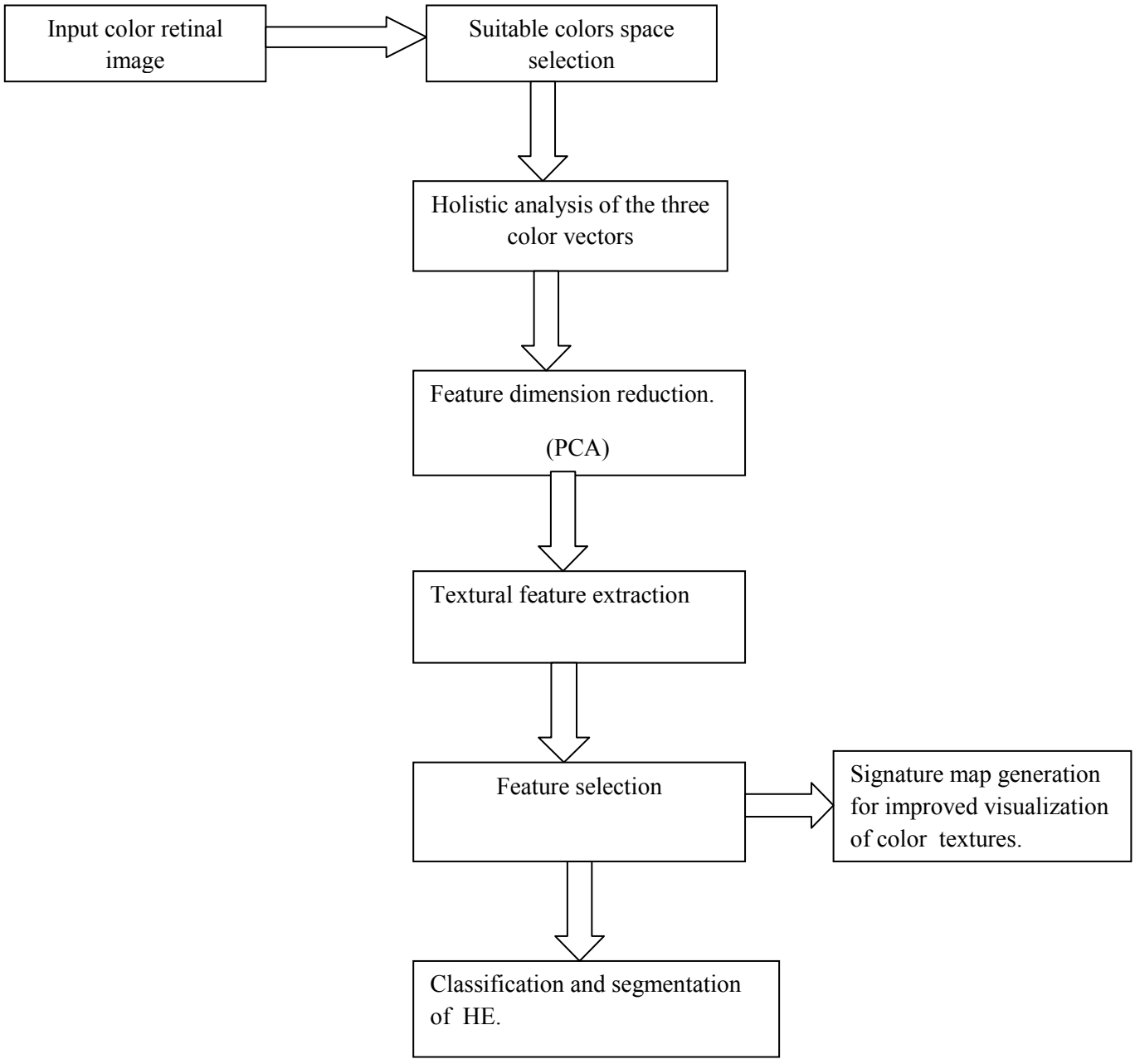

Figure 4.5: Block diagram of the proposed image processing method.

4.3.1. Color space selection

Due to retinal pigmentation and the acquisition process, the retinal images vary largely in luminosity and contrast [6]. As a result, it becomes harder to distinguish retinal features and lesions, thus hindering the automatic segmentation of abnormalities like EXs. Preprocessing

steps to normalize the images and increase the contrast between HEs and the background such as histogram based image normalization and contrast enhancement methods have been applied in many literatures on a selected single channel or serially on multiple channels. However those preprocessing techniques have also a drawback. They always affect the information content held in the multichannel color bands of the original image, which possibly leads to loss of vital information. After testing various preprocessing techniques for a sustainable multichannel feature extraction result, such techniques were omitted from the proposed method as most are prone to significant biases and hence were not robust. Instead a selection of color spaces, which conveys the dominant retinal features in an optimum way than the original RGB color space is found to be helpful for further holistic analysis. For this a set of color spaces such as RGB, HSL, Lab, LUV, CMYK and Ycrbcrr were tested and compared for their efficacy in robust and useful extraction of features (texture descriptors).

In a typical retinal image, the red component is over saturated and has low contrast over the bright regions. The blue component is under saturated and has low contrast over the black regions. Only green part has enhanced contrast over the whole region. This makes the image to have very low contrast which is signified by the grouping of large peaks in a small area on the histogram plot. Fig 4.6 shows the red, green and blue components of a typical retinal image.

Two color spaces, which have enhanced contrast and uniformity for EXs and other retinal structures, were selected for further analysis. These were HSL (hue, saturation and lightness/value/intensity), and GLM' (G-component from RGB, L-component from LUV and inverse Magenta component from CMYK color spaces). The first color space was selected since it is believed to have similarity with human color perception and it is less affected by inter and intra image variations due to various artifacts, hence is potentially helpful for our abnormality

detection scheme. The second color space was chosen based on the scatter matrix result of maximum interclass separablity found in [7].

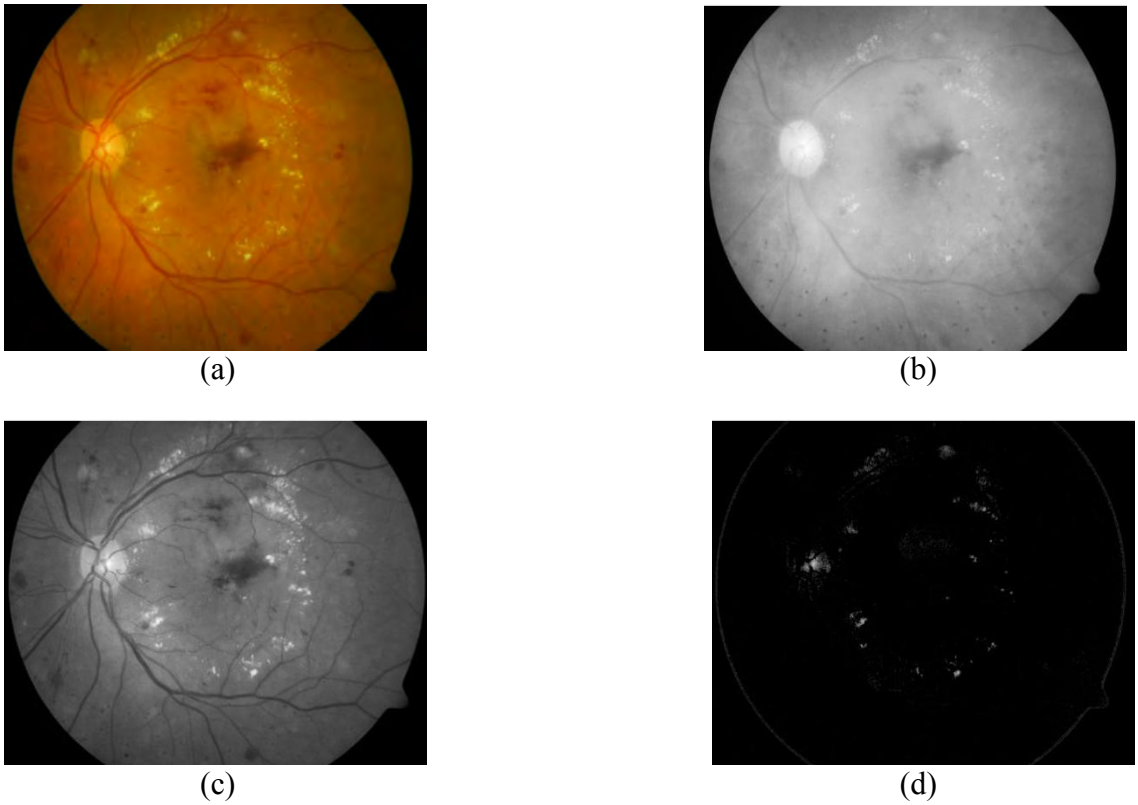

(a) (b) (c) (d)

Figure 4.6: Sample original image with three color components (a), red component (b), green component (c), and blue component (d).

The original RGB image was converted to HSL color using the following formula [9]:

$$H = \arctan\left(\frac{v_2}{v_1}\right), \quad S = \sqrt{{v_1}^2 + {v_2}^2}\ , \quad L = \left(\frac{R+G+B}{\sqrt{3}}\right) \tag{4.1}$$

where:

$v_1 = \frac{(2R-G-B)}{\sqrt{6}}$, and $v_2 = \frac{(R-G)}{\sqrt{2}}$

GLM' color bands for enhancing features of DR

As said before, the green channel of the original color fundus image is commonly used when applying image processing tools to study DRs. The reason is that most methods rely on the color

intensity information as a basis for designing image processing algorithms for color images. The green channel of fundus retinal images shows higher contrast for HEs, for example, and hence often used in HE detection and segmentation [10, 11]. However, a more holistic analysis should essentially be more informative and hence resulting in a more effective analysis of color images. In that regard, in the current work, three representative channels were combined for use in abnormality detection due to DR and OD localization in fundus images. The G-channel from RGB color space was selected based on the above fact: in fundus images, HEs appear brighter than the background, and that is mostly taken up by the green channel. The L channel from the LUV color space was selected as a second channel, since luminosity information has uniformity for EXs and OD [12]. In most fundus images HEs appear yellowish, while background color is red. The inverse magenta channel was selected from CMYK color space as a third channel since it gives great separation with dark red blood vessels and OD (see Fig. 4.7 for example).The scatter matrix of the GLM' color space as calculated in [7] is greater than the RGB, HSV, LUV and Lab color spaces in terms of separating EXs from non EX pixels.

4.3.2. Holistic image processing in the trinion space

The Fourier transform, the Gabor transform, wavelets, the Stockwell (S) transform and many others have been used in various literatures for monochromatic image analysis of gray scale images. The same transforms can be applied in areas of color image processing but only after separating the colors into monochromatic images and analyzing the resulting images serially. The major drawback of such a setting is that separation of color components results in loss of the intrinsic correlation information among the different color bands. Another issue is the higher computational cost involved when analyzing each component separately and trying to correlate each output, which is often not trivial. There are some image processing applications, such as

linear filtering, that are less affected by color separation. But in many other applications, such as texture analysis and pattern recognition, we witness a different scenario. In this regard, designing holistic methods that allow analysis of color images as a single entity/object could be vital.

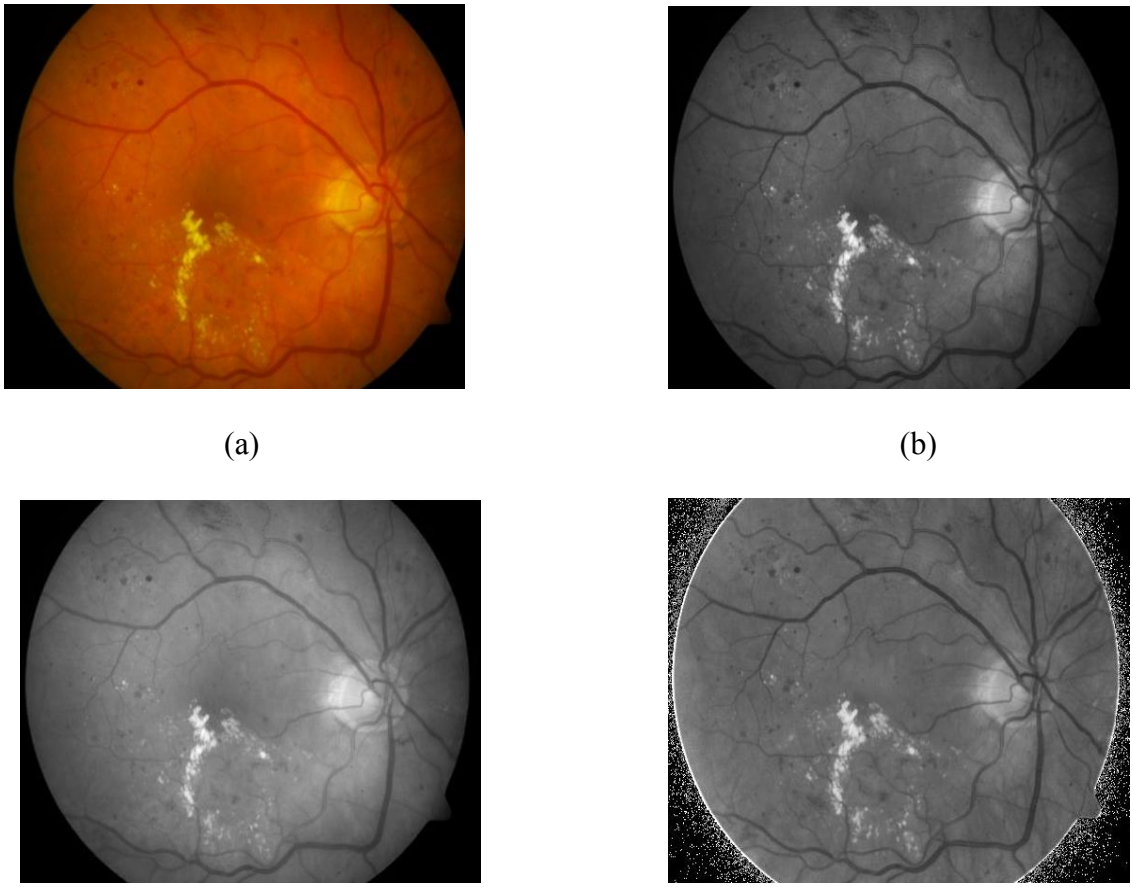

(a) (b)

(c) (d)

Figure 4.7: Sample original image (a), green channel (b), luminance channel (c), and inverse magenta channel (d).

We are interested in robust texture feature based analysis of color retinal images for use in effective classification and segmentation. Visual analysis of textures is often a difficult task especially in medical images where, in general, the texture patterns may be very subtle and their assessment very subjective. Quantitative texture analysis attempts to provide objective metrics and determines neighborhoods around pixels (texture elements) for which the voxel intensities

and spatial relationship between them is used to extract certain quantitative features that characterize the texture of this neighborhood. Statistical approaches are widely employed in texture recognition and description of images [13]. Such methods include, for example, measurement of local image variations to help in contrasting image elements, calculation of auto correlation functions based on spatial frequencies, calculation of correlations to measure image linearity and the like. The traditional way of analyzing color images through separating the monochromatic components misses out the inter-correlation information that is embedded among the monochromes. The task can be accomplished more effectively and efficiently by employing more holistic techniques. In that regard, methods that rely on vectorial representation of color images have recently been proposed and have shown very great promises. One such successful approach uses quaternions for efficient representation of color images and quaternion based integral transforms to effectively analyze color images as a whole by treating the color voxels as vectors [14, 15]. A quaternion is defined with one real and three imaginary components. Interesting properties of quaternion are discussed in detail in literatures [8]. Quaternions have been used to represent three component color images by setting one of the components to zero. However, most color images, including our fundus camera images, have three components and the extra fourth dimension in quaternions creates redundancy in representing such images with additional computational cost. This issue has been discussed in the literature and a solution has been suggested. This is through the use of the three component numbers known by the name trinions [9]. Due to their convenience in representation of three component color images as well as their ability to display full three dimensional color spectra, trinions are adopted as a basis for designing novel segmentation scheme for the retinal images in this thesis.

Trinions have one real term and two imaginary components. A trinion number t is defined as:

$$t = a + ib + jc \tag{4.2}$$

where a, b and c are real numbers, i and j are operators satisfying the following multiplication rules:

$$ii = j,\ jj = -i \text{ and } ij = ji = -1 \tag{4.3}$$

The three base elements [1, i, j] of trinions form an abelian (commutative) group where 1 is the multiplicative identity element. Distinct from quaternions, trinions with the above structure form a commutative ring. Trinions are associative as well as distributive with respect to addition and multiplication [9]. Any trinion number *t* can be expressed as the sum of a real part and a vector part as:

$$t = S(t) + V(t) \tag{4.4}$$

where $S(t) = a$ is the real part and $V(t) = ib + jc$ is the vector part. It can also be written in the following form:

$$t = |t|(cos\,\varphi + \mu sin\,\varphi) \tag{4.5}$$

where $|t| = \sqrt{a^2 + b^2 + c^2}$, $\mu = \frac{V(t)}{|V(t)|}$ and $\varphi = tan^{-1}\left(\frac{|V(t)|}{S(t)}\right)$, $0< \varphi <\pi$ are the amplitude (modulus), the eigen axis and eigen angle (phase) respectively. When $|t| = 1$ it is a unit trinion and when *a=0* it is a pure trinion. More interesting properties of trinions are discussed in the literature [9].

Two working definitions for the trinion Fourier transform (TFT) have been suggested [9]. The TFT of type I and its inverse (ITFT) are given by:

$$T(u,v) = \int_{-\infty}^{\infty}\int_{-\infty}^{\infty} h(x,y)\,(\cos(2\pi(ux+vy)) - \mu_1 \sin(2\pi(ux+vy)))\,dxdy \tag{4.6}$$

$$h(x,y) = \int_{-\infty}^{\infty}\int_{-\infty}^{\infty} T(u,v)\left(\cos(2\pi(ux+vy)) + \mu_2 sin\left(2\pi(ux+vy)\right)\right)dudv \tag{4.7}$$

where *h(x, y)* is generally a trinion valued image function, μ_1 is a unit pure trinion, and μ_2 is a trinion such that the product $\mu_1\mu_2$ =-1. The choice of $\mu_1$and μ_2 is arbitrary. As done in previous studies [9], the choices of $\mu_1$and μ_2 are given by $\mu_1 = \frac{(i-j)}{\sqrt{2}}$ and $\mu_2 = \frac{(-1-i+j)}{\sqrt{2}}$.

There exists a type II TFT in the literature [9]. However, many operations of interest including convolutions and correlations are shown to be easier using the type I TFT than type II TFT [9], and hence the former has been adopted in the current study.

The discrete TFT and its inverse are computed as follows:

$$T(u,v) = \frac{1}{MN}\sum_{x=0}^{M-1}\sum_{y=0}^{N-1} h(x,y)\left(\cos\left(2\pi\left(\frac{ux}{M}+\frac{vy}{N}\right)\right) - \mu_1 \sin\left(2\pi\left(\frac{ux}{M}+\frac{vy}{N}\right)\right)\right) \quad (4.8)$$

$$h(x,y) = \sum_{u=0}^{M-1}\sum_{v=0}^{N-1} T(u,v)\left(\cos\left(2\pi\left(\frac{ux}{M}+\frac{vy}{N}\right)\right) + \mu_2 \sin\left(2\pi\left(\frac{ux}{M}+\frac{vy}{N}\right)\right)\right) \quad (4.9)$$

where

$M \times N$ is the total number of voxels (vectors) present in the selected region of interest (window) of the original image.

u=0,…..N-1, v=1…..M-1, are the discrete frequencies along the horizontal and vertical directions respectively.

The converted RGB color retinal image is mapped to a trinion as: $h(x,y) = H + iS + jV$ in the case of HSV color space, and $h(x,y) = G + iL + jM'$ in the case of GLM' color space. It has already been shown previously that the order of the mapping to a trinion doesn't affect the image analysis [9].

Spatially localized analysis in the selected color space was then performed by computing the TFT over a translating window of size 3x3. Note that after discritization, the TFT was computed using the fast Fourier transform.

4.4. Textural feature extraction for candidate detection and improved visualization

Higher order ’Haralick’ texture features were extracted from TFT transformed image matrix computed over a 3x3 translating window. Note that these features are 'Haralick' only in form. For example, we do not compute the GLCM as Haralick did but we instead compute novel features in the trinion space and finally use Haralick formulas to quantify our textures using different texture descriptors.

Feature dimension reduction

Before computing these features, Principal Component Analysis (PCA) was applied on each 3 ×3 localized TFT transformed image, each resulting in a trinion valued output in the new PCA space each of which is a 3 × 3 matrix in our case. This step was needed in order to reduce some redundancy in our multi-channel data. The PCA algorithm is freely available on the Algorito website at http://algorito.com/algorithm/principal-component-analysis-pca-transform. Then each value of the resulting 3x3 matrix was normalized between 0 and 1 and these are the probability density functions used to compute the texture features. Note that each texture features were extracted component wise on the trinion valued PCA matrix. Then the computed feature is assigned to the central voxel value in that window. The step is then repeated across all voxels that are included in the selected region of interest over the image. The final signature map results were generated as a color using the trinion valued local texture descriptors.

Nine different Haralick features were computed: Sum-mean, Variance, Energy (Angular Second Moment), Correlation, Homogeneity, Contrast, Entropy, Cluster shade, and Cluster prominence, and tested for their efficacy in uniquely quantifying different objects in our retinal samples [13, 16].

Sum-mean=$0.5\sum_{u=1}^{3}\sum_{v=1}^{3}(u(p(u,v))+v(p(u,v)))$ (4.10)

Variance=$0.5\sum_{u=1}^{3}\sum_{v=1}^{3}[(u-\mu)^2p(u,v)+(v-\mu)^2p(u,v)]$ (4.11)

Energy = $\sum_{u=1}^{3}\sum_{v=1}^{3}p(u,v)^2$ (4.12)

Correlation= $\sum_{u=1}^{3}\sum_{v=1}^{3}\frac{(u-\mu_x)(v-\mu_y)p(u,v)}{\sigma_x\sigma_y}$ (4.13)

Homogeneity= $\sum_{u=1}^{3}\sum_{v=1}^{3}\frac{p(u,v)}{1+(u-v)^2}$ (4.14)

Contrast= $\sum_{u=1}^{3}\sum_{v=1}^{3}(u-v)^2\log(p(u,v))$ (4.15)

Entropy=$-\sum_{u=1}^{3}\sum_{v=1}^{3}p(u,v)\log(p(u,v))$ (4.16)

Cluster shade=$\sum_{u=1}^{3}\sum_{v=1}^{3}(u+v-\mu_x-\mu_y)^3p(u,v)$ (4.17)

Cluster prominence=$\sum_{u=1}^{3}\sum_{v=1}^{3}(u+v-\mu_x-\mu_y)^4p(u,v)$ (4.18)

where:

$p(u,v)$ is the normalized spectral value (which can be assumed probability density function) obtained after application of PCA on the TFT transformed image matrix,

$\mu=\frac{1}{9}\sum_{u=1}^{3}\sum_{v=1}^{3}p(u,v)$ is mean of the matrix

$\mu_x=\sum_{u=1}^{3}u\sum_{v=1}^{3}p(u,v)$ is the sum of row mean,

$\mu_y=\sum_{v=1}^{3}v\sum_{u=1}^{3}p(u,v)$ is the sum of column mean,

$\sigma_x^2=\sum_{u=1}^{3}(u-\mu_x)^2\sum_{v=1}^{3}p(u,v)$ is sum of row variance, and

$\sigma_y^2=\sum_{v=1}^{3}(v-\mu_y)^2\sum_{u=1}^{3}p(u,v)$ is the sum of column variance.

These features were used to generate the final signature maps, which allow differentiating between areas corresponding to HE, H, OD, and other regions that have clinical significance related to DR. The performance of signature maps generated using the different texture features was compared and assessed accordingly through qualitative comparison of the signature maps against the available ground truths.

4.5. Segmentation of abnormal retinal structures

4.5.1. Coarse segmentation

The efficacy of the proposed signature map generation scheme has been tested using the various publicly available datasets with respect to its usefulness in visual enhancement of pathological features due to DR, localization of OD in the presence and absence of glaucoma, as well as in detection of EXs. The generated signature map is used to relieve latent image signals on the original images which have clinically important textural features. This is achieved by selecting the most relevant and non redundant textural feature that best suits for our purpose. The available data sets contain images with different abnormality types and a thorough investigation has been carried out to identify those textural features with better performance in terms of accuracy and robustness in detecting/identifying the abnormalities and other structures of interest relevant to DR.

Analyzing the signature maps

Based on the available ground truth, features maps with best performance were first selected based on their level of accuracy in classifying different structures in the retinal images. In order to quantify the classification accuracies, the trace metric, given by eqn. (4.19), was computed. The metric J estimates the class separablity of pixels (EXs versus non-EXs, for example) using within-class ($\boldsymbol{S_w}$) and between-class ($\boldsymbol{S_b}$) scatter matrices as follows:

$$J = trace(\boldsymbol{S_b S_w}^{-1}) \quad (4.19)$$

where:

trace is a mathematical operator which provides the sum of diagonal elements of a square matrix.

$$\boldsymbol{S_b} = (\mu_{ex} - \mu_{non-ex})\,(\mu_{ex} - \mu_{non-ex})^T \quad (4.20)$$

$$\boldsymbol{S_w} = \boldsymbol{S_{ex}} + \boldsymbol{S_{non-ex}} \quad (4.21)$$

μ_{ex} and μ_{non-ex} are the means of the EX and non-EX classes respectively, estimated using the corresponding training sets.

$\boldsymbol{X_{ex}}$ and $\boldsymbol{X_{non-ex}}$ are the training sets for EX and non-EX classes respectively.

N and M are the total number of X_{ex} and X_{non-ex} that are present in the training set respectively.

$$\mu_{ex} = \frac{1}{N}\sum_{i=1}^{N} \boldsymbol{X_{ex}^i} \quad (4.22)$$

$$\mu_{non-ex} = \frac{1}{M}\sum_{i=1}^{M} \boldsymbol{X_{non-ex}^i} \quad (4.23)$$

$\mathbf{S_{ex}}$ and $\mathbf{S_{non-ex}}$ are the scatter matrices of each class:

$$\boldsymbol{S_{ex}} = \frac{1}{N}\sum_{i=1}^{N}(\boldsymbol{X_{ex}^i} - \mu_{ex})\,(\boldsymbol{X_{ex}^i} - \mu_{ex})^T \quad (4.24)$$

$$\boldsymbol{S_{non-ex}} = \frac{1}{M}\sum_{i=1}^{M}(\boldsymbol{X_{non-ex}^i} - \mu_{non-ex})\,(\boldsymbol{X_{non-ex}^i} - \mu_{non-ex})^T \quad (4.25)$$

A higher value of J indicates that the classes are more separated while members within each class are closer to each other. Additionally a set of experiments were done on the resulting signature maps by changing some parameters of the algorithm. The following cases were investigated:

- Effect of the feature extraction with and without the application of PCA.
- Effect of applying PCA on the absolute value of the transformed image matrix.
- Effect of localizing window size.
- Background subtraction with varying window size.

In each case the performance of the resulting signature map was assessed accordingly through qualitative comparison of the signature maps against the available ground truths.

For normalization, each component (channel) was divided by its maximum. However, in so doing the occurrence of some wrong peak value or noise signal could suppress the true image information in the resulting color images. In addition variation of those maximum values from image to image or in the same image with different regions causes unwanted color variations in the signature maps. To solve this problem, the value located at the point of the top 95% of the distribution is taken as the nominal maximum. All features greater than the nominal maximum in the feature space were clipped to the nominal maximal value, that is, the top 5% of distribution are trimmed. Then all values are divided by the maximal values. In addition for contrast enhancement of low intensity values logarithmic transform technique was applied on each channel.

4.5.2. Exudate segmentation

Figure 4.8 presents a schematic diagram of the proposed method that combines a SVM classifier with signature map color information to enable precise segmentation of HEs, classification of abnormal retinal images due to DR, and visual enhancement of major retinal structures. The method is comprised of two major stages. First training was done based on SVM with optimal texture features of 2312 EX and 3109 non-EX pixels. Then its result was fused with the color information of the previously generated signature map which is computed from the best texture feature. The SVM classifier is used to estimate candidate bright lesion regions. However since the SVM classifies some bright non lesion regions as lesions, color information from the signature map is incorporated for fine segmentation of HEs. Fine segmentation of HEs from the

candidate bright regions is done by setting an optimum threshold values and rules based on the observed color information (hue and saturation) of these lesions on the generated signature map.

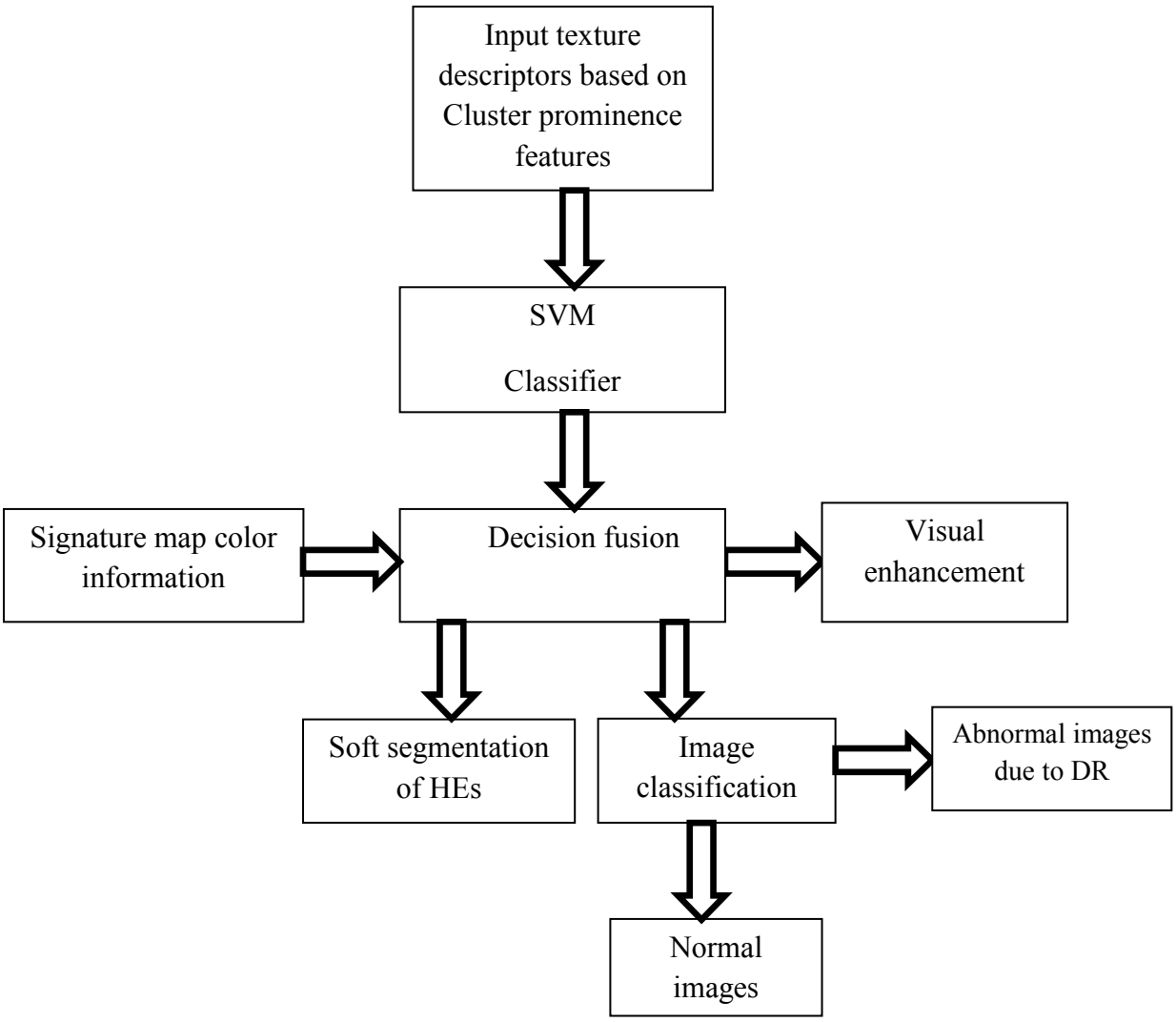

Figure 4.8: Block diagram of the proposed image segmentation and classification scheme.

- **Classification using SVM**

SVM is a statistical learning method based on structural risk minimization (SRM). It can map the input vector X into a high dimensional feature space by choosing a nonlinear mapping kernel [17, 18]. Thus the basic idea of applying SVMs for solving classification problems can be stated as follows:

- ✓ Transform the input space to higher dimension feature space through a non-linear mapping function and,
- ✓ Construct the separating hyper plane with maximum distance from the closest points of the training set.

A binary SVM decision function can be written as:

$$F(X) = \sum_{i \in s} \alpha_i Y_i \; K(X_i, X) + b \qquad (5.26)$$

where X is the feature vector to be classified, i indexes the training sample, α_i are Lagrange multipliers, S is a set of indices for which X_i is a support vector, i.e., a vector for which $\alpha_i \neq 0$ after optimization, α_i and b (bias) are fit to the data to maximize the margin, Y_i is the label $[-1, 1]$ of training sample i, and K is the kernel function [17]. A serious problem with nonlinear kernel SVMs is their complexities of classification which are high when a large number of support vectors are needed [19]. There are many kernels that can be used, such as linear, polynomial, radial basis function (RBF) and sigmoid.

We have used linear kernel and a regularization parameter C=1 in our experiment. The support vectors, α_i and b were all automatically obtained by the SVM training procedure. The performance of the selected SVM classifier was then quantified based on its sensitivity, specificity and the overall accuracy on the test (training) samples.

- **Feature extraction**

Based on the results we have observed in the signature map generation (presented in the next chapter), the following feature vectors were extracted and tested by the SVM classifier for the purpose of bright lesion estimation.

- o Cluster prominence feature value from the three channels.
- o Amplitude map of the cluster prominence feature vector.

- Standard deviation over 5x5 region on the amplitude map of the cluster prominence feature vector.
- Mean value over 5x5 region on the amplitude map of the cluster prominence feature vector.
- Edge feature based on Soble edge operator over 5x5 region on the amplitude map of the cluster prominence feature vector.
- Features based on trinion edge detection method.

- **Selected features**

After testing the results of the SVM classifier, four features were used for further analysis. Those features are Cluster prominence feature values from the three channels and amplitude map of Cluster prominence feature vector.

Decision fusion

In this stage we develop a dynamic tresholding algorithm and incorporate it with the SVM classifier result for precise segmentation of HEs. The algorithm is developed based on the results that are observed in the signature map analysis stage (these results are presented in the next chapter). For separating HE pixels from non HE bright pixels on the original image the result of the SVM classifier is combined with color information of the signature map. As demonstrated in Fig. 4.9, the proposed decision fusion algorithm eliminates non HE pixels from the SVM result by incorporating the chromaticity (hue and saturation) information of HEs from the signature map. For this purpose, two parameters, α and β, are used and set as dynamic segmentation threshold values. This is used for eliminating false positive results by the SVM classifier. A set of dynamic segmentation threshold values, α and β, were tested and optimal ones are chosen based on their performance for use in the proposed HE segmentation scheme.

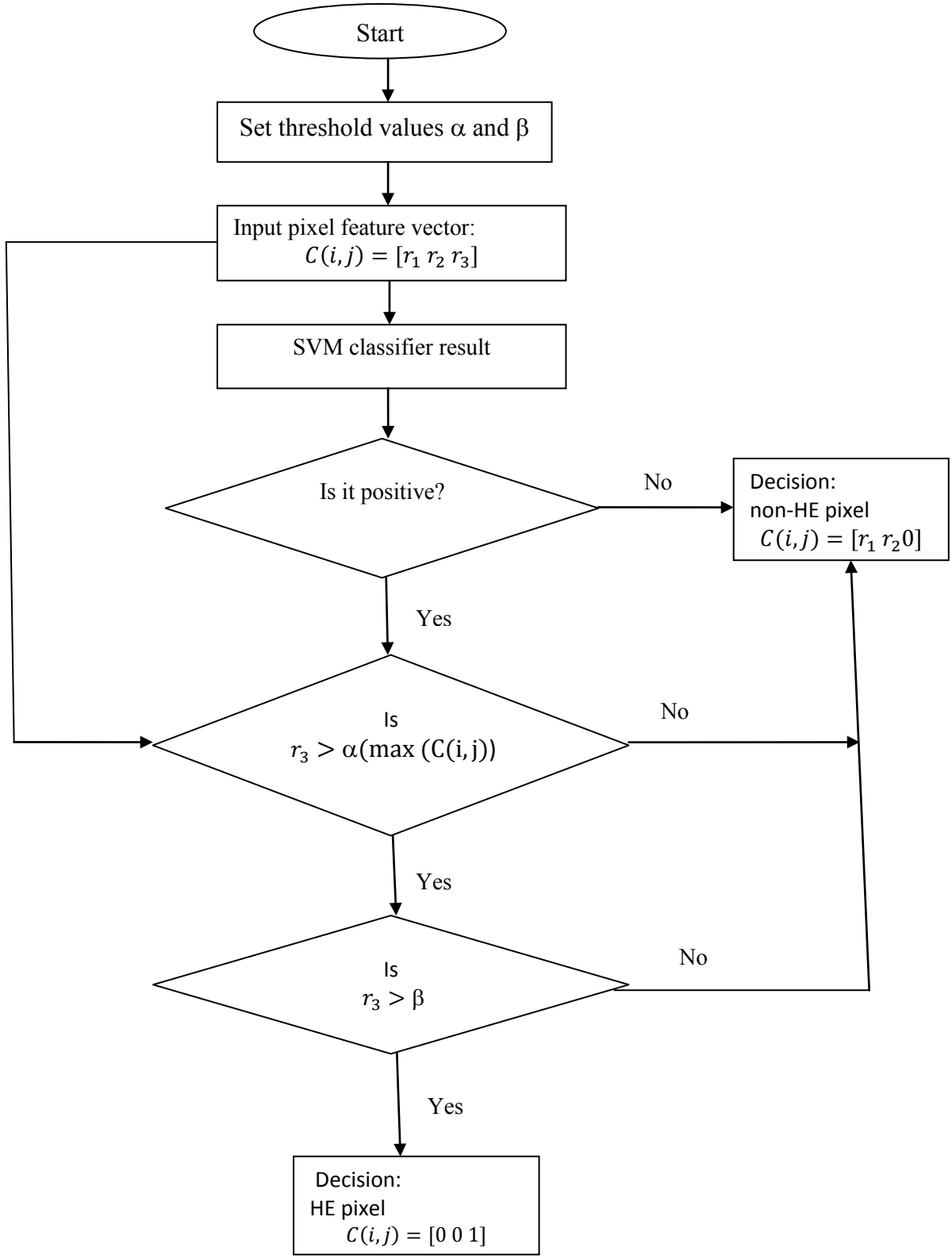

Figure 4.9: Flow chart for the decision fusion algorithm.

In general the rules and assumptions that are used in the decision fusion process can be stated as follows:

- The result of the SVM classifier is assumed as estimator of bright areas on the image based on their luminance value. Hence false positives are eliminated by the knowledge of chromaticity and saturation values of HE pixels from the signature map.
- HE pixels have blue white color on the signature map. This chromaticity information is incorporated to eliminate non lesion bright regions.
- Saturation value for HE is set and used to further eliminate false positives.

The efficacy of the proposed soft segmentation scheme is tested for use in precise segmentation of HEs, identification of abnormal images due to DR, and improved visualization of color textures. Performance evaluation is carried out based on ground truth information for HEs that is available in the data sets. Note that the proposed image processing algorithm in this thesis has been implemented in Matlab (Matlab 2010b).

References

1. P. J. Saine and M. E. Tyler, Fundus Photography Overview, Ophthalmic Photographers Society. Available online: http://www.opsweb.org, Website Referenced on Jan. 10, 2014.
2. P. J. Saine, Fundus Photography: Fundus Camera Optics, Ophthalmic Photographers Society. Available online: http://www.en.wikipedia.org, Website Referenced on Jan. 10, 2014.
3. T. Kauppi, V. Kalesnykiene, J. Kamarainen, L. Lensu, I. Sorri, A. Raninen, R. Voutilainen, H. Uusitalo, H. Kalviainen and J. Pieti, DIARETDB1 diabetic retinopathy database and evaluation protocol, pp. 1-18, 2010.
4. T. Kauppi, V. Kalesnykiene, J. Kamarainen, L. Lensu, I. Sorri, H. Uusitalo, H. Kalviainen, and J. Pieti, DIARETDB0: Evaluation Database and Methodology for Diabetic Retinopathy, pp. 1-17, 2008.
5. K. M. Kade, Fundus Image Acquisition Techniques with Data base in Diabetic Retinopathy, IJERA, 3(2), pp. 1350-1362, 2013.
6. I. Jamal, M. A. Usman, and A. Tariq, Retinal image preprocessing: background and noise segmentation, TELKOMNIKA, 10(3), pp. 537-544, 2012.
7. H.-C. LU and G.-L. Fang, An effective framework for automatic segmentation of hard exudates in fundus image, J. Circuit Syst. Comp, 22(1), 2013.
8. D. Assefa, L. Mansinha, K. F. Tiampo, H. Rasmussen, and K. Abdella, Local quaternion Fourier transform and color image texture analysis, Sig Proc., 90(6), pp. 1825-1835, 2010.
9. D. Assefa, L. Mansinha, K. F. Tiampo, H. Rasmussen, and K. Abdella, The trinion Fourier transform of color images, Sig Proc., 91(8), pp. 1887-1900, 2011.
10. C. I. Snchez, M. Garca, A. Mayo, M. I. Lopez, and R. Hornero, Retinal image analysis based on mixture models to detect hard exudates, Med. Image Anal., 13(4), pp. 650-658, 2009.
11. M. G. F. Eadgahi and H. Pourreza, Localization of hard exudates in retinal fundus image by mathematical morphology operations, Int. Conf. Comput. Knowledge Eng., pp. 185-189, 2012.
12. G. B. Kande, P. V. Subbaiah, and T. S. Savithri, Feature extraction in digital fundus images, J. Med. Bio. Eng., 29(3), pp. 122-130, 2009.
13. D. Assefa, H. Keller, C. Menard, N. Laperriere, R. J. Ferrari, and I. Yeung, Robust texture features for response monitoring of glioblastoma multiforme on T1-weighted and T2-FLAIR

MR images: A preliminary investigation in terms of identification and segmentation, Med. Phys., 37(4), pp. 1722-1736, 2010.

14. S. J. Sangwine and T. A. El, Hypercomplex auto and cross-correlation of color images, IEEE Image Proc., pp. 319-322, 1999.
15. S. –C. Pei, J. –J. Ding, and J. –H. Chang, Efficient Implementation of Quaternion Fourier Transform Convolution and Correlation by 2D Complex FFT, IEEE Trans. On Sig. Proc., 11(49), 2001.
16. J. M. Mendel, Tutorial on higher-order statistics (spectra) in signal processing and system theory: Theoretical results and some application, 2000.
17. A. Osareh, Comparative exudate classification using support vector machines and neural networks, Proc. Int. Conf. Medical Image Computing and Computer-Assisted Intervention-Part II, Springer, Verlag, London, UK, pp. 413-420, 2002.
18. C. J. C. Burges, A tutorial on support vector machines for pattern recognition, Datamin. Knowl. Discov., Vol. 2, pp. 121-167, 1998.
19. K. Wisaeng, N. Hiransakolwong, and E. Pothiruk, Automatic Detection of Retinal Exudates using a Support Vector Machine, Applied Medical Informatics, Vol. 32, pp. 33-42, 2013.

Chapter five

5. Results and discussion[1]

5. 1. Optimal feature map selection for segmentation of retinal images

Based on a qualitative analysis against the available ground truths, signature maps generated based on three features namely: cluster prominence, sum mean, and variance, computed in the GLM' and HSL color spaces were found to be superior to the rest features in terms of uniquely identifying different objects in the retinal samples under consideration. In order to evaluate the classification accuracy of the proposed method in terms of separating HE and non-HE pixels, Table 5.1 presents the scatter matrix (the J index) values for cluster prominence, sum mean and variance features computed on both GLM' and HSL color spaces. The table also includes computed metric results for RGB, YLQ, HSL, GLM', YCbCr, and Lab color spaces. For this experiment, 1009 EX pixels and 2095 non-EX pixels were manually selected to analyze the class separablity of EX and non-EX pixels. For each image, the EX training set is made up by pixels belonging to small isolated EXs as discussed in the previous chapter. Their characteristics can represent the rest of EXs in the image. Additionally, these type of EXs can be found in all fundus images with HEs, even in the earliest stages of DR. The EXs training set is obtained from the available ground truth. As shown in Table 5.1, cluster prominence feature computed over the GLM' color space offered the highest index and hence this is the feature used for optimal segmentation of the retinal images (particularly the HEs).

[1] Parts of the results presented in this chapter have been published recently on the proceedings of the 7th ICT annual conference, Addis Ababa, June 06, 2014.

Table 5.1: Class separablity quantitative metric of various color models and texture descriptors

Color model	Texture descriptor	Scatter matrix (J)
GLM'	Sum mean	5.81
HSL	Sum mean	5.4
GLM'	Variance	5.63
HSL	Variance	5.13
GLM'	Cluster prominence	13.6
HSL	Cluster prominence	9.8
RGB		2.91
YLQ		2.91
HSL		2.98
GLM’		4.14
YcbCr		2.92
Lab		2.99

5.2. Signature map results

Signature maps generated using cluster prominence computed using the GLM' color space showed improved results over the other features. It correctly differentiated the OD from the HE. Even in the presence of glaucoma, OD localization was done successfully by this feature. In the absence of DR, the signature map correctly localized the OD. Fig. 5.1 presents computed feature maps for representative fundus images acquired from four patients treated for moderate non proliferative DR. In each case HEs (white bluish) were correctly identified by the proposed scheme. The ODs (cyan color) were also correctly detected as well.

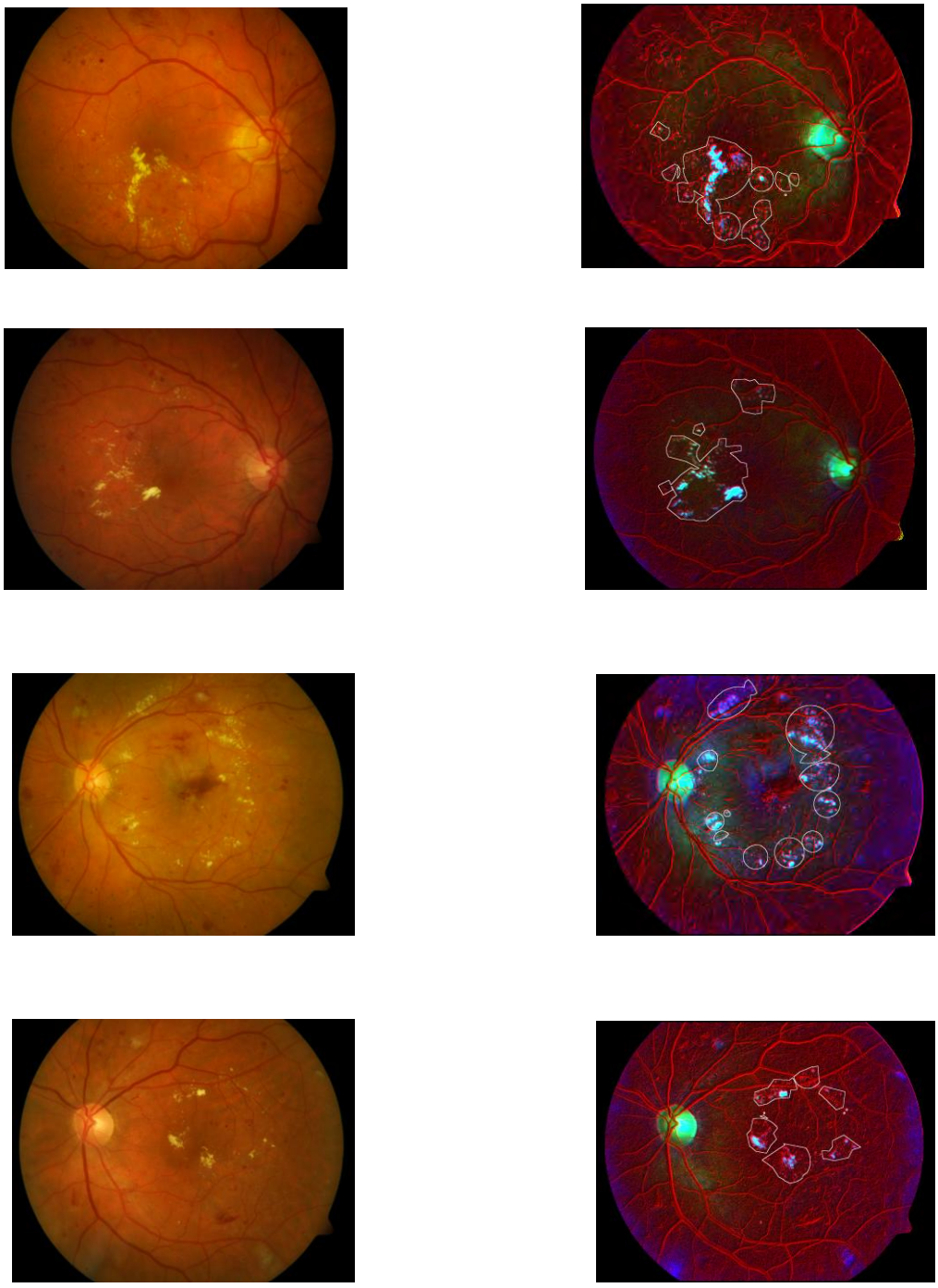

Figure 5.1: HE detection results: original images with moderate non proliferative DR (1st column) and the respective signature maps generated using the proposed scheme (2nd column). White lines are the ground truths that denote HEs.

In Fig. 5.2 results are presented to demonstrate the efficiency of the proposed scheme in OD localization. In both the normal as well as the Glaucoma cases, very compact signatures maps were generated for the ODs (cyan color) well distinct from the background. In this stage only qualitative analysis was done by comparing signature map results with the available ground truths.

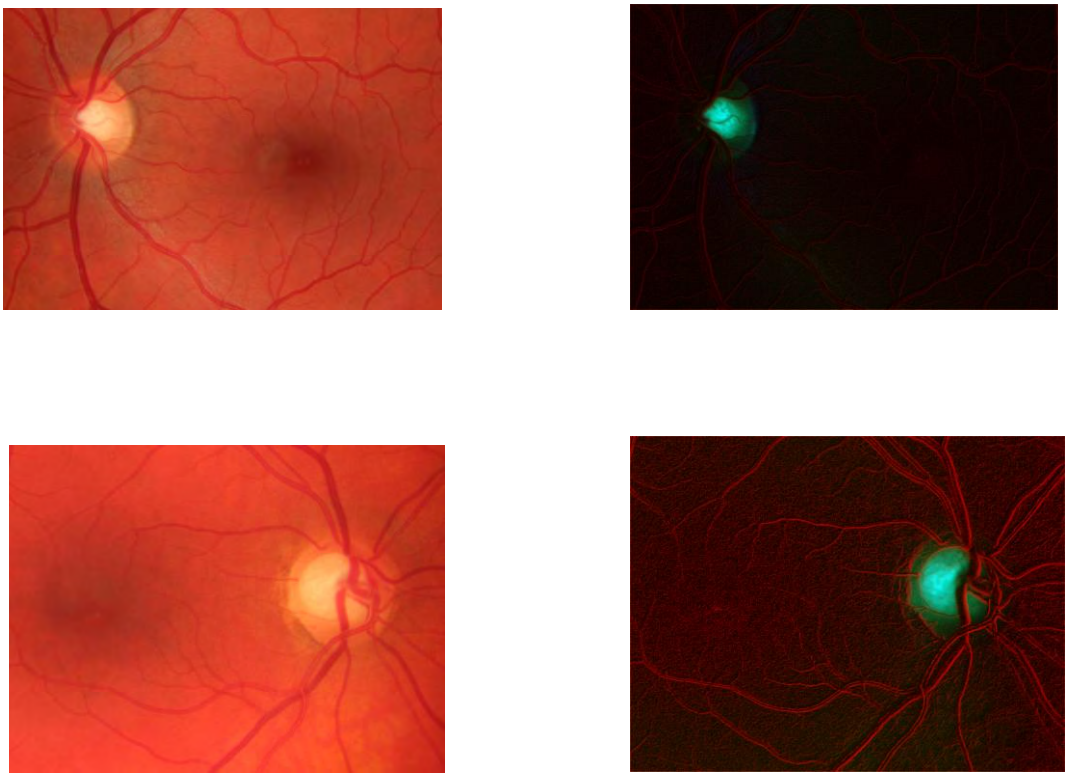

Figure 5.2: OD localization results: original color fundus images (1st column) and feature maps (2nd column) showing compact signatures for the OD. The upper image was a normal case while the bottom one was a patient eye due to Glaucoma.

The problem with most feature based algorithms for detection of EXs is presence of false detection because some pixels with similar color to the EXs belong to OD and edges of blood vessels [1]. Preliminary signature map results have showed that the method proposed in this

thesis has the potential of solving this problem. A distinct textural feature of those abnormality markers was revealed in the generated signature maps. Generally, there is a good agreement between the signature maps generated and the available ground truth. Thus the proposed multi channel texture feature map can be used as a powerful tool for image segmentation and classification purposes. In the following subsection sample experimental results are presented. Detail descriptions of the signature map results with the number of test images that are used from the dataset are also incorporated.

5.2.1. Experiments and discussion

Experiments were held on a total of 214 sample original retinal images. As demonstrated in Table 5.2, images of healthy subjects and patients treated for DR and glaucoma are included in the sample set. Good quality images with different background color and illumination as well as bad quality images due to poor illumination and noise are also included in the test sample. Qualitative analysis was done to investigate the potential and limitations of the algorithm by observing the resulting signature maps of all test images that are included in the sample set. The experimental tests have showed that the algorithm achieved best results by using 3x3 translating window size and by applying PCA on the TFT transformed image matrix. The resulting signature maps were found very helpful for visual enhancement of pathological features due to DR, localization of the OD and EXs robustly.

- **HE detection and OD localization**

As demonstrated in Fig. 5.1 EXs appear in blue white color on the generated signature maps distinct from other structures and the rest of the background. The signature maps offered considerable visual enhancement and distinction of HEs and the OD. A total of 125 abnormal retinal images due to DR were taken during the experiment and the respective signature maps

robustly detected the HE pixels in a unique color. Generally the tolerance of the algorithm for change in background color and illumination conditions was found very satisfactory. Our results showed that, the third component of the signature maps in particular was found most informative for our EX identification purpose. This is for example demonstrated in Fig. 5.3.

Table 5.2: Sample data set of retinal images used for testing signature map results

Standard retinal image data set	Number of images used for testing	Description of images
DB00	45	9-normal and 36-non proliferative DR
DB01	89	5-normal and 84- non proliferative DR
HRF	45	15-normal, 15-glaucoma, and 15-non proliferative DR
DRIVE	15	15- non proliferative DR
STARE	20	2-normal and 18-non proliferative DR

In addition to the visual enhancement of HEs and the OD, the signature maps give important information for setting a threshold value of features which can be used as a decision boundary for separating EXs from other regions and thereby automating the segmentation process. Figure 5.4 demonstrates this fact; it is the plot of cluster prominence features (2^{nd} and 3^{rd} channels) extracted for 600x750 region of a test image. The plot was generated based on the ground truth information of HEs and non HE pixels in the selected region. As seen in the figure, pixels which

are HEs have feature values which can be easily separated from the background by setting a threshold decision boundary. Experiments have shown that the 3rd channel gives the highest interclass separation of classes for HEs and the OD. The second channel also gives a good separation between background pixels and pixels due HEs and the OD but its ability to separate the HEs from the OD is less satisfactory.

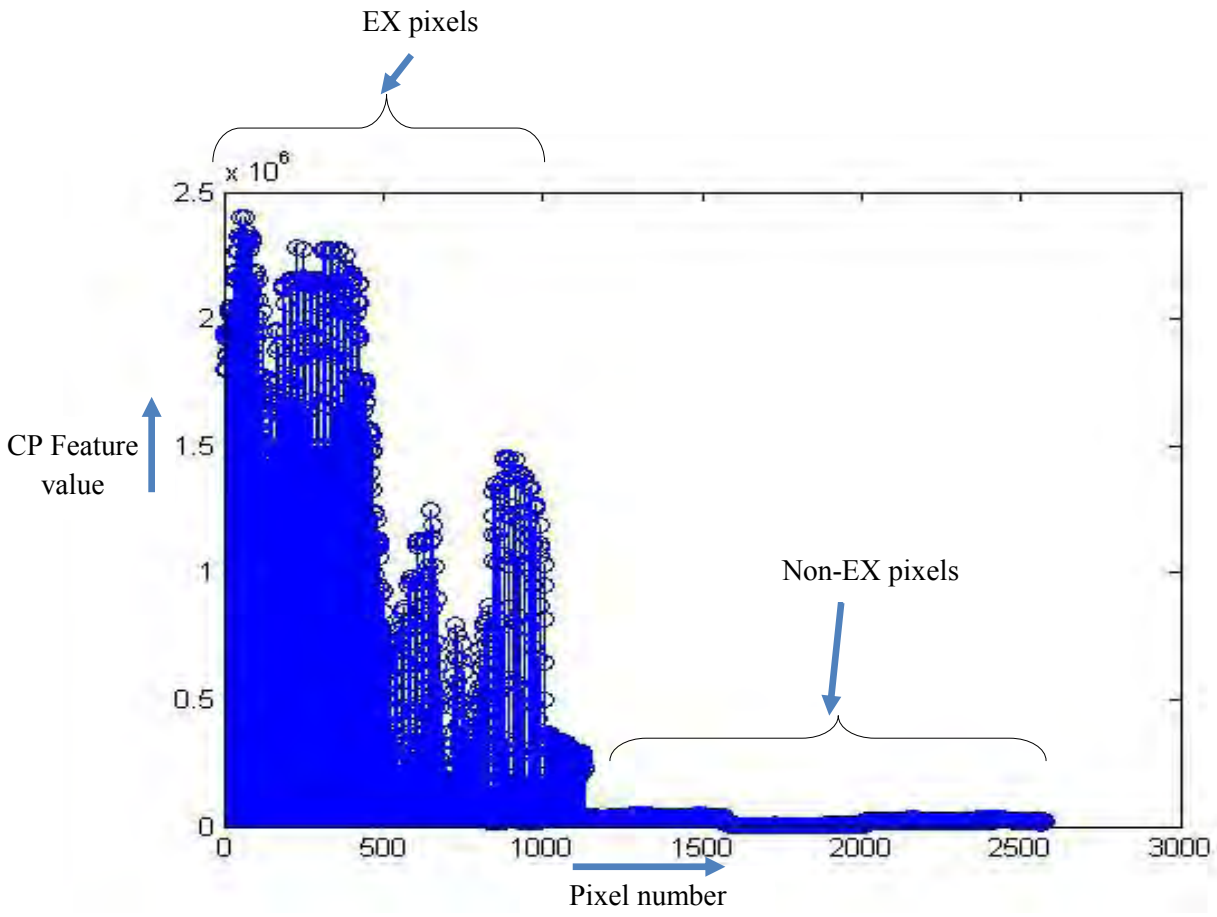

Figure 5.3: A plot of cluster prominence feature in the third component for 1009 exudates and 1565 non exudate pixels.

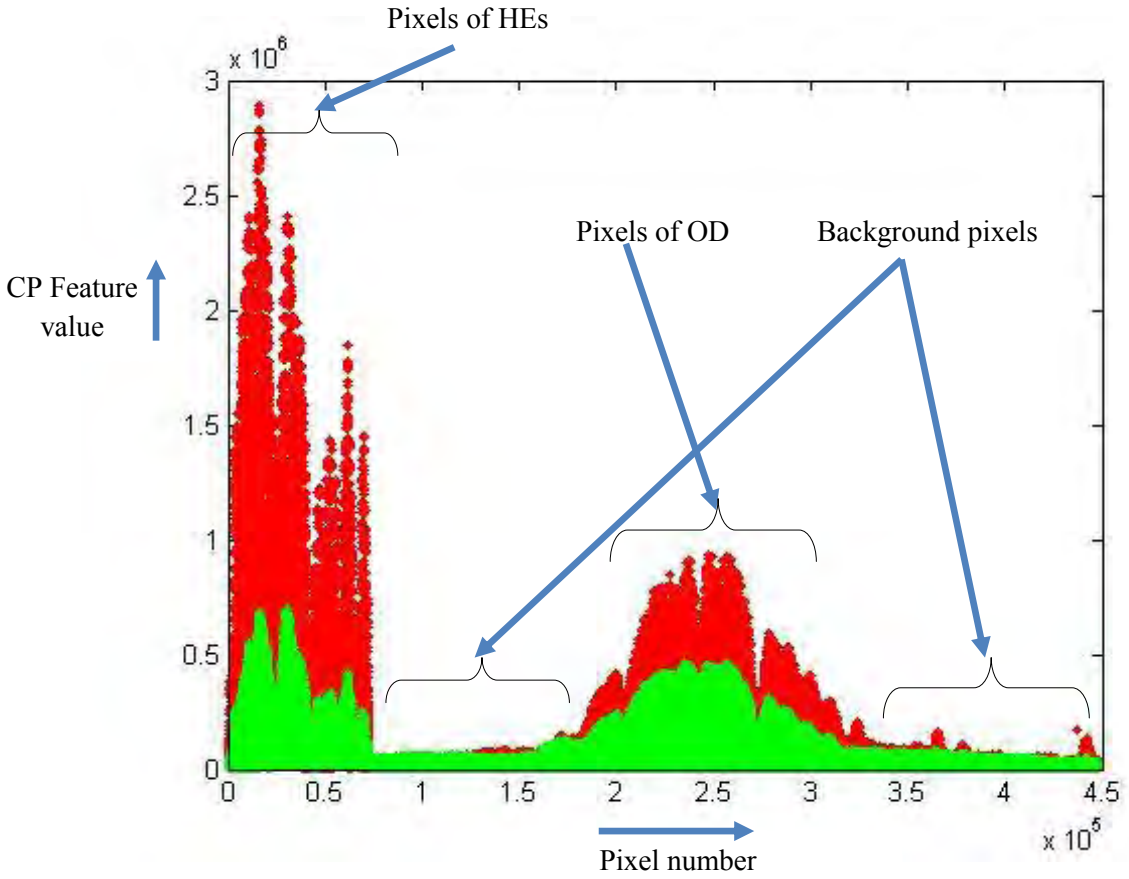

Figure 5.4: A plot of cluster prominence feature for randomly selected HE and non HE pixels based on ground truth information: red indicates the feature value of the third channel and green indicates feature value of second channel. The first channel is not plotted since it has very low feature value when compared with the others.

OD localization experimental results were observed for 25 normal images, 15 abnormal images due to DR and 15 abnormal images due to glaucoma. Generally well distinct signature maps were observed for the OD (cyan color) for all images in the sample set. Figure 5.5 presents signature map results of three normal (non DR) retinal images with different background colors and taken under different illumination conditions. In all cases it is evident that the OD appears in a unique and consistent color with great separation from the back ground structures. Notice that

the retinal images taken for the experiments in this thesis were taken under different illumination conditions and had different background colors.

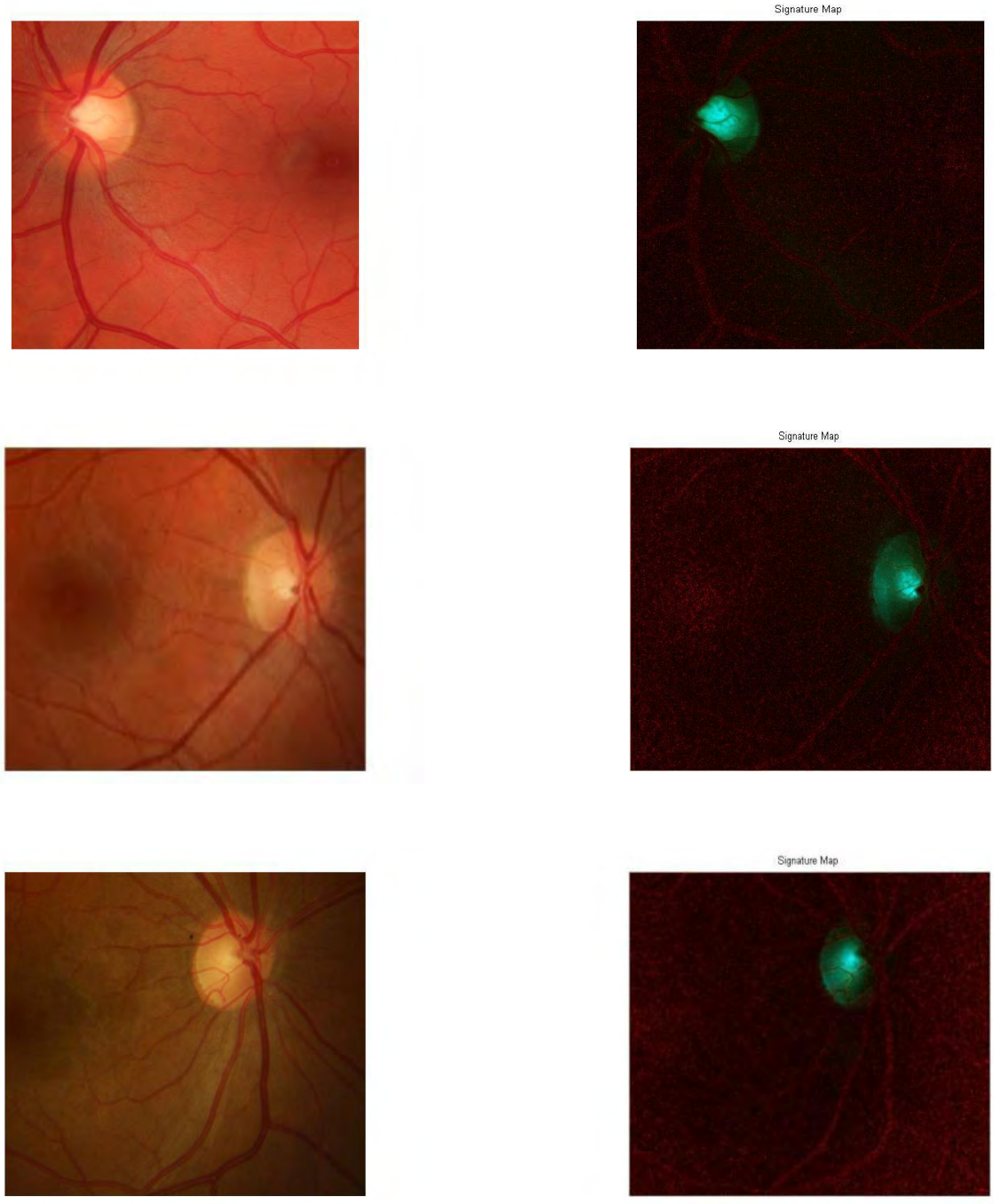

Figure 5.5: Generated signature maps for normal retinal images which have different illumination and background colors. Original images (1st column) and computed signature maps (2nd column).

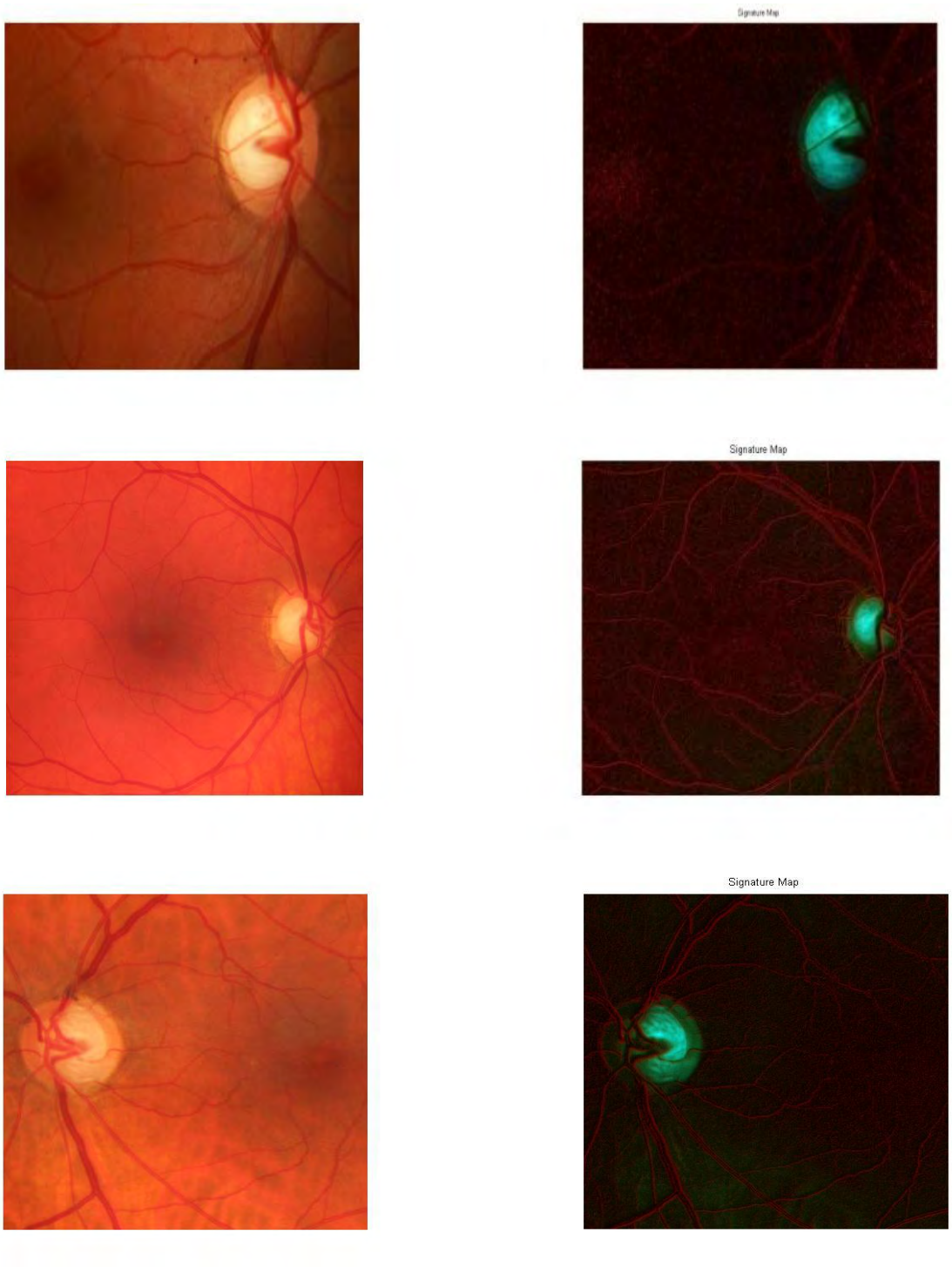

Figure 5.6: Generated signature maps in the presence of glaucoma; original images with different illumination and background color (1st column), signature maps extracted from cluster prominence (2nd column).

In the presence of glaucoma the signature maps have revealed enhanced textural information for the OD and structures inside it such as the optic cup and the major vertically emerging blood vessels, which usually are essential information for glaucoma detection. Fig. 5.6 presents signature map results of three abnormal retinal images due to glaucoma. In each case clinically important textural features that can help for diagnosis of glaucoma such as the shape, shallowness and width of OD including the morphology of the major blood vessels were revealed in enhanced way on the resulting signature maps. In addition the color of the OD remains the same as the normal cases.

- **Limitations**

Generally there is a good agreement between the generated signature maps and the ground truth. However, there are still rooms for improvement particularly regarding the application of the proposed scheme on images captured under very poor illumination and higher noise conditions. One solution can be excluding the fundus areas with poor luminance accompanied by better noise suppression mechanisms [2] before computing the features.

5.3. System performance evaluation

The automated image processing scheme, which is proposed in section 4.5.2, combines the results of SVM classifier with the signature map color information based on the decision fusion algorithm presented in Fig. 4.9. The experimental results that we have seen so far clearly demonstrate that the proposed method offered great promises in automatic segmentation of HEs, classification of abnormal retinal images due to DR and visual enhancement of retinal images. Quantitative analysis has been carried out to evaluate the performance of the proposed system. Two different criteria were set up in this regard: pixel-based criteria and image-based criteria. The first criterion examines the ability of the proposed algorithm for pixel base detection (i.e.

segmentation) of HEs while the second one evaluates algorithm's ability to distinguish (i.e. classify) between images containing HEs and healthy retinas. In the case of the pixel based criteria, 24168 HE pixels and 24186 non HE pixels taken from 65 retinal images with non proliferative DR have been taken. For the image based criteria, 7 normal and 30 abnormal retinal images with HE present on them have been taken.

Four commonly used performance matrices were computed for the sake of performance evaluation: sensitivity, specificity, positive predictive value, and accuracy as described below.

Sensitivity (SE): it is the proportion of actual positives which are predicted correctly. Mathematically, sensitivity can be defined as:

$SE = \frac{TP}{TP+FN}$, where TP represents true positives (the total number of pixels that are detected as HE by the proposed method while HEs are actually present) and FN represents false negatives (the total number of pixels which are detected as non-HE by the proposed method while HEs are actually present).

Specificity (SP): is the proportion of actual negatives which are predicted negative. It can be defined as:

$SP = \frac{TN}{TN+FP}$, where TN represents true negatives (the total number of pixels that are detected as non-HE by the proposed method while HEs are actually absent) and FP represents false positives (the total number of pixels that are detected as HE by the proposed method while HEs are actually absent).

Positive predictive value (PPV): measures the probability of actual positives which are predicted positive. It is defined as:

$$PPV = \frac{TP}{TP+FP}$$

Accuracy (ACC): it is the probability to correctly identify individuals, i.e., it is the proportion of true results, either true positive or true negative. It is computed as:

$$ACC = \frac{TP+TN}{TP+TN+FP+FN}$$

Further quantitative analysis was done on the pixel based criteria to demonstrate and compare results. The proposed algorithm has two parameters, α and β, which determine threshold values to consider a pixel as HE. In order to study their influence on the performance of the algorithm, the number of true positives (TPs), true negatives (TNs), false positives (FPs) and false negatives (FNs) that are present on the test samples were computed for different values of α and β. Sixteen simulation sets were tested and optimum segmentation thresholds were selected based on results.

The following sets of parameter values were tested:

$\alpha = [0.8, 0.85, 0.95, 1]$ and $\beta = [0.1, 0.15, 0.2, 0.3]$

Optimum values of α and β were selected from the above sets by comparing the results of different performance measures. The accuracy of HE segmentation scheme can be measured in terms of sensitivity and specificity by comparing the obtained results against the ground truth outline of the EXs. However in [3] the authors mentioned that specificity was not an informative measure in the pixel-based criterion. They argued that the number of true negatives (TNs) was generally much higher than that of false positives (FPs) in retinal images. As a result, even if EXs detection is inaccurate, specificity values could still be high. Alternatively, the positive predictive value (PPV) was regarded as a more significant criterion to evaluate the performance of the system. Thus we assess the performance based on the pixel-based sensitivity (SE) and the

PPV, which measures the probability that a detected region is really an EX. In addition the Free-Response Operating Characteristic (FROC) curve [4] was also used to analyze the sensitivity of the system against false positive rate (see Fig. 5.7).

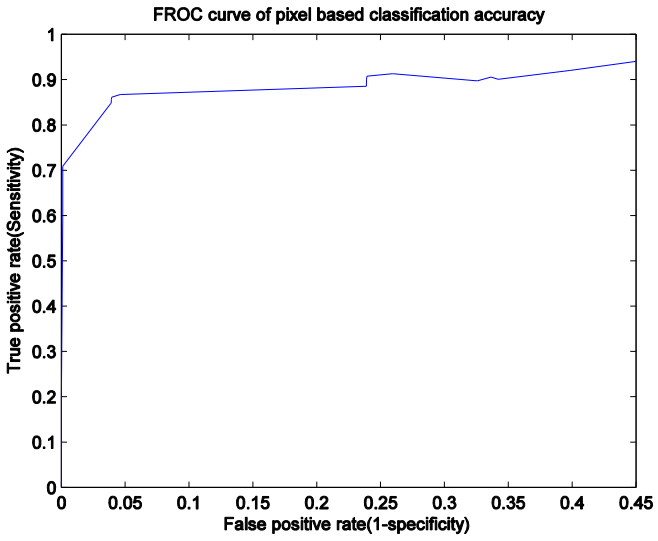

Figure 5.7: ROC curve

Accordingly, for pixel based criteria best performance measures, i.e. SE=86.08%, SP=96.06% and PPV=94.47%, were achieved at parameter values, α=0.8 and β=0.2. The performance for the other parameter values that are tested for being a segmentation thresholds are presented in Table 5.3. For image based classification the algorithm classifies all the 7 normal retinal images correctly, while it fails to detect only 1 abnormal image from a total of 30 abnormal test images included in the test set. Generally using the parameters α=0.8 and β=0.2, optimum image based performances, i.e., SP=100%, PPV=100% and SE=96.67% were achieved. The general accuracy of the algorithm was found 92.65% for pixel based criteria while it was 97.3% for image base criteria. It is widely believed that SE and SP values of greater than 80% and 90% respectively are acceptable for clinical applications of such a system. That means our method is good enough to be used in a clinical setup.

Table 5.3: Results of the proposed HE segmentation scheme for different segmentation tresholding values

α	β	SE	SP	PPV
0.8	0.1	0.9204	0.6010	0.6674
0.8	0.15	0.9129	0.7406	0.7321
0.8	0.2	0.8608	0.9606	0.9474
0.8	0.3	0.8479	0.9606	0.9471
0.85	0.1	0.8878	0.6579	0.6874
0.85	0.15	0.9077	0.7606	0.7577
0.85	0.2	0.8593	0.9606	0.9466
0.85	0.3	0.8471	0.9606	0.9466
0.95	0.1	0.9055	0.6636	0.6894
0.95	0.15	0.9013	0.7609	0.7566
0.95	0.2	0.8559	0.9606	0.9471
0.95	0.3	0.8469	0.9540	0.9320
1	0.1	0.8872	0.6742	0.6918
1	0.15	0.8854	0.7618	0.7541
1	0.2	0.8472	0.9616	0.9466
1	0.3	0.7088	1.0000	1.0000

In Fig. 5.8 HE segmentation results of four representative images which have EXs on them are presented. In all cases the HEs were very well detected on the respective maps (pure blue colors). Results for three retinal images that have no HE pixels on them are presented in Fig. 5.9. In each case it is evident that the resulting images have no sign of HE (pure blue color). In addition to its

segmentation and classification capabilities, the proposed method also gives enhanced contrast in color for the OD and the background regions.

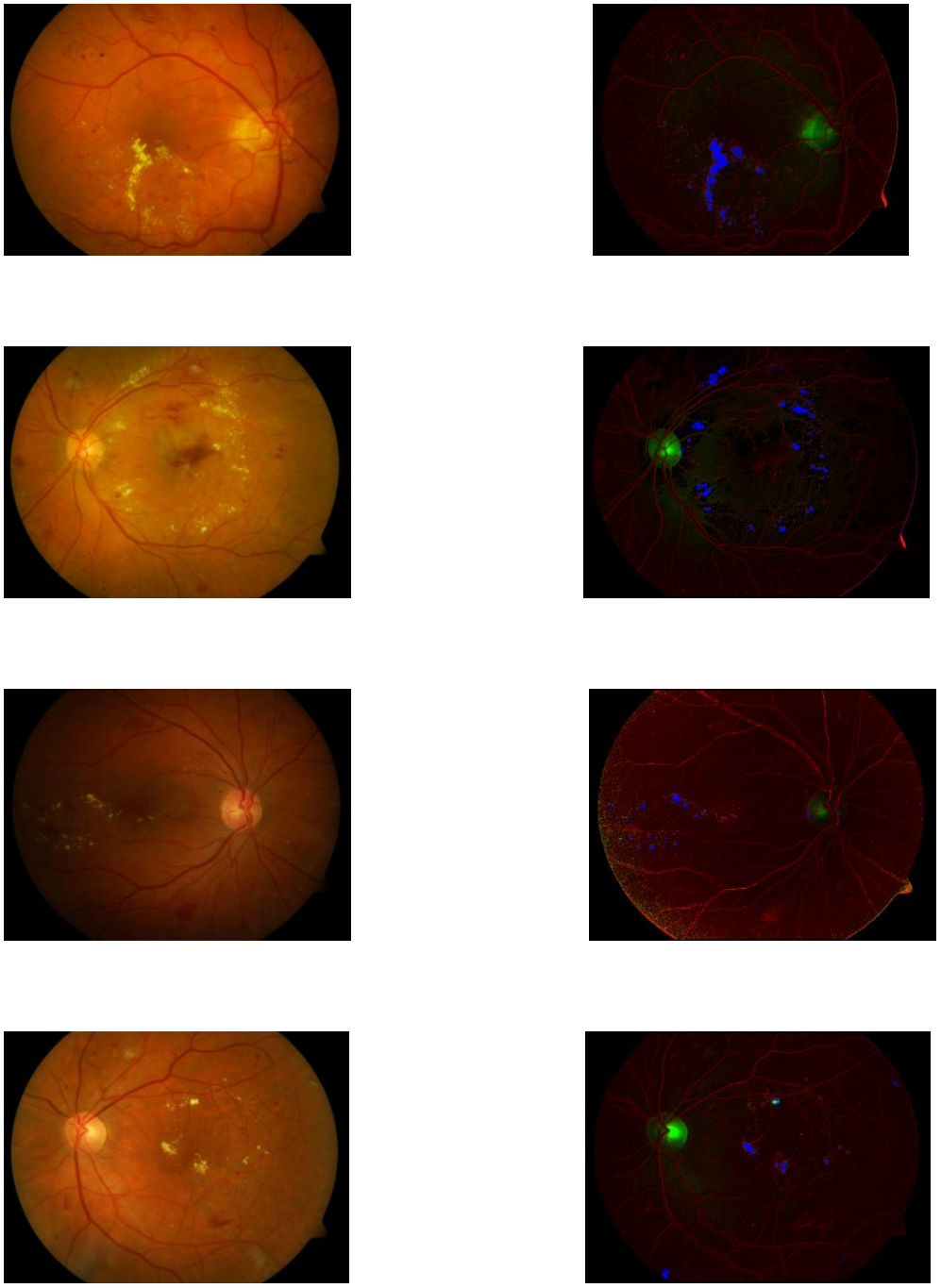

Figure 5.8: HE segmentation results; Original retinal images having HE on them (1st column) and results after segmentation of HE pixels with a pure blue color (2nd column).

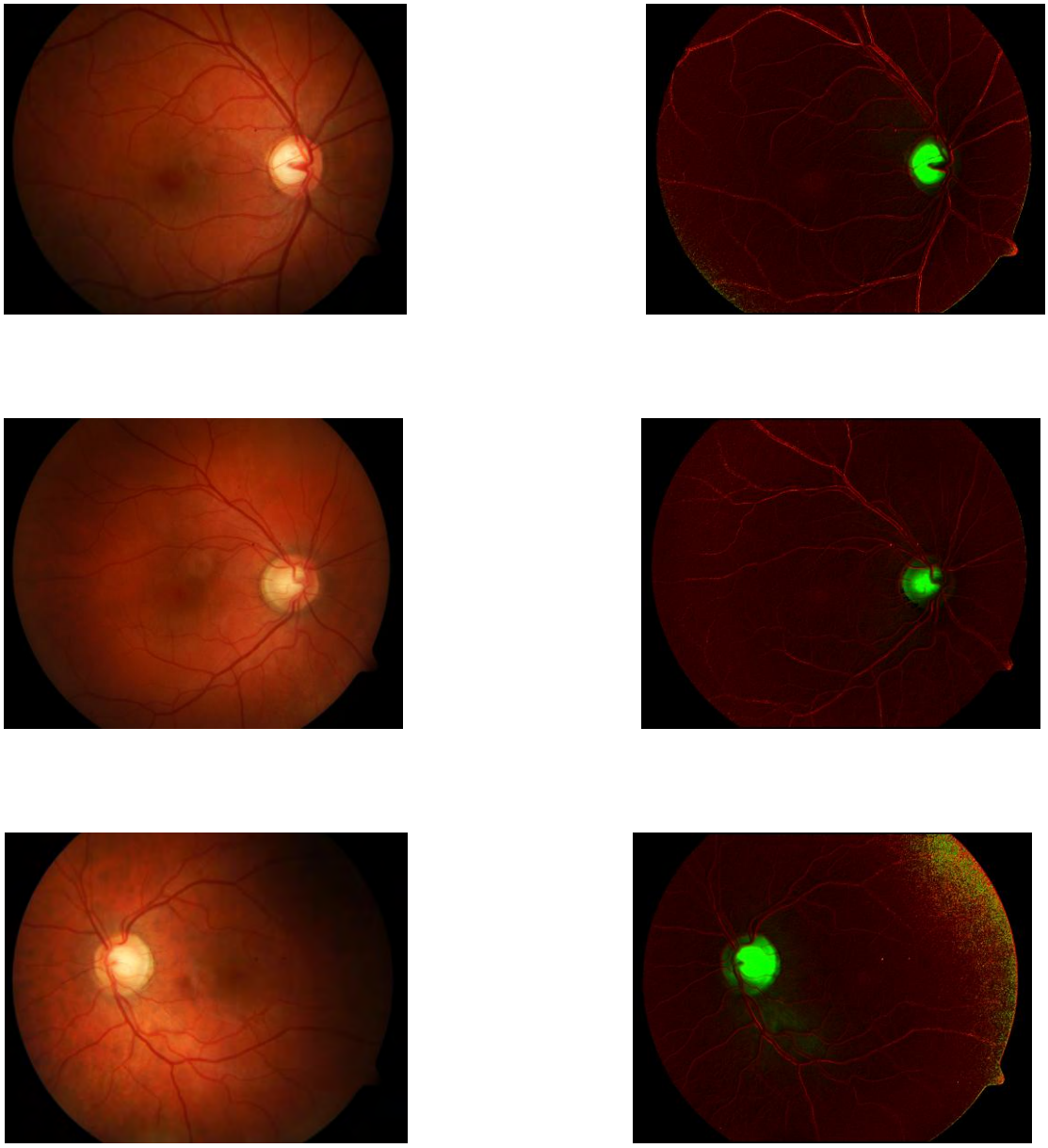

Figure 5.9: Results for retinal images that have no exudates on them; original images (1st column) and results after segmentation (2nd column).

5.4. Comparison and discussions

One of the main challenges in the automatic identification of HEs is the wide variability of fundus color among different subjects. Earlier works partially avoided this problem by using only one of the image color bands [5-9]. However, color information is an important feature that

can be used to distinguish among different lesions. The proposed algorithm makes use of the holistic color information during the processing stage and achieves better performance in the image segmentation stage. Various analysis techniques to characterize the features of HEs are suggested in the literatures. Preprocessing techniques have also been used to enhance the relevant features of retinal lesions. Simple approaches such as histogram equalization often fail due to wide variability in color, illumination, and contrast. Such sensitivity to colors is often regarded as the major drawback of histogram based approaches including histogram equalization and histogram specification for use in retinal image analysis. In the current work contrast or illumination are improved at the expense of an intrinsic characteristic texture feature that resides in the image. The algorithm uses the holistic color information and extracts relevant higher order features for contrast enhancement and segmentation of lesions due to HEs. The process is adapted to the intrinsic characteristics of the retinal images. Additionally, the class separablity of EX and non-EX pixels in this new multichannel feature space is increased compared with other color models.

Selecting the appropriate training and testing set is also important since it directly affects the performance of the algorithm. The proposed approach in this thesis entails using different training and testing data sets selected from the available images in order to take into account the large inter-image variability. Hence performance of the algorithm is evaluated prospectively using an independent database of retinal images containing variable characteristics in order to investigate its robustness and its suitability for usage in a clinical environment. The retinal images in the data set contain different clinical signs such as EXs, hemorrhages, MAs and/or CWs. Inclusion of images containing all these structures during our experiment enables us to assess the robustness of the algorithm in the presence of other lesions.

References

1. N. P Ward, S. Tomlinson, C. J Taylor, Image analysis of fundus photographs -The detection and measurement of exudates associated with diabetic retinopathy, Ophthalmol., Vol. 96, pp. 80-86, 1989.
2. I. Jamal, M. A. Usman, and A. Tariq, Retinal image preprocessing: background and noise segmentation, TELKOMNIKA, 10(3), pp. 537-544, 2012.
3. M. García, C. I. Sanchez, M. I. Lopez, D. Abasolo and R. Hornero, Neural network based detection of hard exudates in retinal images, Comput. Meth. Progr. Biomed. Vol. 93, pp. 9-19, 2009.
4. D. P. Chakraborty, J. Beutel, H. L. Kundel, and R. L. Metter, The FROC, AFROC and DROC variants of the ROC analysis, Handbook of Medical Imaging, SPIE Press, Vol. 1, pp. 771-796, 2000.
5. H. Li, O. Chutatape, Automated feature extraction in color retinal images by a model based approach, IEEE Trans. Biomed. Eng., 51(2), pp. 246–254, 2004.
6. R. Philips, J. Forrester, and P. Sharp, Automated detection and quantification of retinal exudates, Graefe's Archive for Clinical and Experimental Ophthalmology, 231(2), pp. 90-94, 1993.
7. T. Walter, J. C. Klein, P. Massin, and A. Erginay, A contribution of image processing to the diagnosis of diabetic retinopathy—detection of exudates in color fundus images of the human retina, IEEE Trans. Med. Imaging, 21(10), pp. 1236-1243, 2002.
8. N. P. Ward, S. Tomlinson, and C. J. Taylor, Image analysis of fundus photographs—the detection and measurement of exudates associated with diabetic retinopathy, Ophthalmology, Vol. 96, pp. 80-86, 1989.
9. G. Gardner, C. Leverton, S. Young, J. Lusty, F. Dunstan, and D. Owens, Automatic detection of diabetic retinopathy using an artificial neural network: a screening tool, J. Ophthalmol., 80(11), pp. 940-944, 1996.

Chapter six

6. Conclusion and recommendations

6.1. Conclusion

A novel approach has been proposed in this thesis for use in color retinal image processing which uses a holistic representation of the color images in the three (trinion [1]) space and applies trinion based Fourier transforms to extract useful imaging features. A suitable color space transformation and a way of extracting robust higher order features are also included in the method. Results have been analyzed to demonstrate the efficiency of the proposed methods for the following two major applications:

i. Visual enhancement of the major anatomical and pathological features in retinal images.
ii. Automatic segmentation of HEs and classification of abnormalities due to DR.

For the first application the potential of signature maps extracted from various higher order statistical features were analyzed. Enough number of image samples with wider range of degree of difficulties have been used for assessing the potentials of the signature maps in extracting useful information pertinent to DR studies. Focus was given to detection of EXs, OD localization, and partly to characterization of retinal blood vessels as well as hemorrhages. Signature maps were also tested to reveal clinically important information in the presence of glaucoma. Our results have showed that the texture maps extracted from Cluster prominence feature, computed over GLM' color space, revealed enhanced textural information which can be used for OD localization in the presence of EXs, for detection of HEs and for image based classification of abnormalities in the retina. It also revealed enhanced textural information for the

OD and structures inside it such as the optic cup and the major vertically emerging blood vessels, which is essential information for glaucoma detection. Accurate detection of this retinal morphology has great clinical significances for diagnosis and prognosis of patients.

Precise segmentation of HEs from the background and other bright areas was done by fusing the results of SVM classifier applied on the generated color signature maps. The performance of the algorithm was analyzed in terms of statistical measures such as sensitivity, specificity, positive predictive value and accuracy; each was measured for pixel base and image base criteria. Generally the algorithm achieved SE of 86.06%, SP of 96.06, PPV of 94.475% and ACC of 92.65% for pixel base segmentation of HEs, while it achieved SE of 96.67%, SP of 100% , PPV of 100%, and ACC of 97.3% for image base classification of abnormalities due to HEs. The preliminary results indicated that the proposed method yielded an acceptable performance with promising potentials to be included in computer aided intelligent health care systems for diagnosis of eye diseases due to DR and glaucoma.

6.2. Recommendations

Although the results presented in this study have demonstrated the effectiveness of the proposed method, there are still rooms for improvement for the scheme to be used in automatic retinal image analysis systems. Other than detection of EXs, the OD, blood vessels and other structures presented in the results section of this thesis, there are still other lesion types considered useful in DR studies including hemorrhages, Microaneurysms and cotton wool spots and the proposed algorithm should take into account of these structures. Furthermore, HE classification has to be improved further by considering other clustering techniques. The system developed so far is capable of detecting maculopathy. It has to be further developed to include detection of more severe retinopathies.

In order to make general conclusions regarding the diagnostic values of the proposed algorithm, assessment on a larger data set could be required. That would make the results more representative of the performance expected in a clinical setting. Furthermore, extensive validation study must be carried out on the results presented in this thesis which might require an observer study.

It is largely believed that, the changes in the shape and size of the OD can be used to detect glaucoma [2]. The proposed method gives enhanced visualization for those features. However the method has to be further improved to precisely detect optic cup part of the disc so that changes in the disc to cup ratio can be used to detect presence of glaucoma.

Segmentation of retinal vessels can further be used for a number of purposes. The retinal vascular toruosity is shown to become a predictive factor for cardiovascular diseases and diabetes [3]. The changes in retinal vascular toruosity might be used as biomarkers of disease severity. Finding a new technique to analyze and quantify toruosity by considering vessel segment's width awaits further investigation.

References

1. D. Assefa, L. Mansinha, K. F. Tiampo, H. Rasmussen, and K. Abdella, The trinion Fourier transform of color images, Sig. Proc., 91(8), pp. 1887-1900, 2011.
2. D. A. Godse and D. S. Bormane, Automated Localization of Optic Disc in Retinal Images, Advanced Computer Science and Applications, 4(2), 2013.
3. A. Osareh and B. Shadgar, Automatic blood vessel segmentation in color images of retina, Int. J. Sci. Tech. Trans. Eng., 33(B2), pp. 191-206, 2009.